Oxy-polishing of gas from chemical looping combustion: Fuel-nitrogen transformation and model-aided gas purity optimization

Citation for the original published paper (version of record):
Mei, D., Lyngfelt, A., Mattisson, T. et al (2025). Oxy-polishing of gas from chemical looping combustion: Fuel-nitrogen transformation and
model-aided gas purity optimization. Chemical Engineering Journal, 509.
http://dx.doi.org/10.1016/j.cej.2025.161267

Chemical Engineering Journal 509 (2025) 161267

Contents lists available at ScienceDirect

Chemical Engineering Journal

journal homepage: www.elsevier.com/locate/cej

Oxy-polishing of gas from chemical looping combustion: Fuel-nitrogen transformation and model-aided gas purity optimization

Daofeng Mei [a,b,c,*], Anders Lyngfelt [a], Tobias Mattisson [a], Carl Linderholm [a]

[a] Division of Energy Technology, Department of Space, Earth and Environment, Chalmers University of Technology, Gothenburg 41296, Sweden
[b] Department of Energy and Environment, Instituto de Carboquímica (ICB-CSIC), Miguel Luesma Castán 4, Zaragoza 50018, Spain
[c] College of Engineering, Huazhong Agricultural University, Wuhan, 430070, People's Republic of China

ARTICLE INFO

Keywords:
Carbon capture
Greenhouse gas
Combustion
Chemical looping
Reactor model

ABSTRACT

Chemical looping combustion (CLC) is a carbon capture technology for heat, power and hydrogen production. This work focuses on fuel-nitrogen transformation in fuel reactor and its further conversion in oxy-polishing step of CLC system. A 100 kW CLC pilot equipped with an oxy-polishing chamber (called POC) was used to perform experiment study and a zero-dimensional reactor model combining elementary reaction kinetics was developed and used for oxy-polishing simulation and reaction path analyses. An ilmenite and a manganese ore called Sinaus were used as oxygen carriers, and a coal and a coal-biomass mixture are the fuels in the CLC tests. It was found that in the fuel reactor, part of the fuel-nitrogen was converted to NO and the rest remained as NH_3 which was then oxidized to NO in the POC. The concentrations of HCN and NO_2 were negligible in the fuel reactor and POC. According to the simulation, when the oxygen excess is too low it is difficult to reach 1150–1200 °C which are temperatures needed for oxidizing the unconverted fuel gases. In a reference case, a high conversion was reached when the overall oxygen ratio was above 1.03 and temperature above 925 °C. With a fuel reactor temperature of 950 °C, the oxygen demand needed could be up to around 8 %. Based on the model, optimal geometrical designs of the POC were proposed. With a gas residence time of 3 s in the POC, it was possible to decrease the content of impurities (O_2, H_2, CO, NO, CH_4) to 3.3 %.

1. Introduction

Given the fact that the global warming is getting worse as a result of CO_2 emissions from the extensive use of fossil fuels, a transition to renewable energy is needed [1]. However, the phasing out of fossil fuels will take time [2]. During this transition, efficient technologies that can capture CO_2 from fossil emissions will be needed. Furthermore, the carbon budget for a warming of maximum 1.5 °C will likely be exhausted around 2029. So, to meet this target, all fossil CO_2 emissions made from 2030 and onwards need to be removed from the atmosphere using negative emission technologies [3]. One of the most important options for negative emissions is Bio-Energy with Carbon Capture and Storage (BECCS).

Chemical looping combustion (CLC) is a novel technology [4,5], which inherently captures CO_2 at low energy penalty and can be used to capture of fossil CO_2 emissions as well as BECCS. The CLC concept can be sourced back to 1950 s when Lewis and Gilliland patented a technique for pure CO_2 generation [6], while the process first got its name "chemical looping combustion" in late 1980 s by Ishida et al. [7]. The first successful operation of a chemical looping combustor pilot was in 2003 [8,9]. Since then, chemical looping research has undergone a rapid development [10–13]. Today, around 50 CLC pilots with a thermal power range of 0.3 kW_{th}-5 MW_{th} have been in operation [12,14–18], where the 5 MW_{th} granted by an EU-China CHEERS project has been successfully operated for more than 60 h with lignite and petcoke with low oxygen demand, <3% [18,19].

Chemical looping combustion uses a fluidized bed as fuel reactor and another fluidized bed as air reactor, as seen in Fig. 1, and these two reactors are interconnected through fluidized loop seals which prevent contact between the gases in the air and fuel reactors [20,21]. The circulation is normally driven by a gas at high velocity in e.g., the air reactor, that forces the particles of the bed material upwards. The elutriated particles can be collected by a cyclone and led to the fuel reactor. Another option, likely more appropriate for commercial scale, is

* Corresponding author at: Division of Energy Technology, Department of Space, Earth and Environment, Chalmers University of Technology, Gothenburg 41296, Sweden.
E-mail address: dmei@icb.csic.es (D. Mei).

https://doi.org/10.1016/j.cej.2025.161267
Received 20 October 2024; Received in revised form 3 February 2025; Accepted 4 March 2025
Available online 5 March 2025

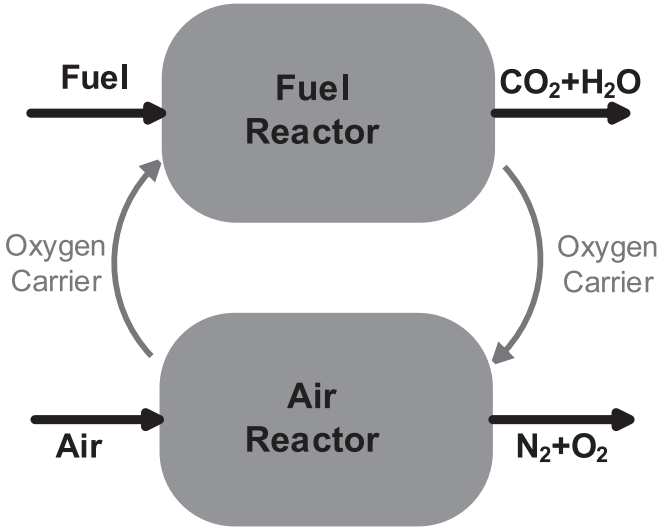

Fig. 1. Schematic of chemical looping combustion.

to collect the wall downflow of the air reactor riser and lead this to the fuel reactor [22]. Oxygen for fuel combustion is transferred from the air reactor to the fuel reactor through oxygen carrier which is usually oxides of transition metals [23]. The oxygen carrier particles constitute the bed material of the interconnected reactors. The oxygen carrier is reduced in the fuel reactor while providing oxygen for fuel combustion and is then returned to the air reactor where it takes up oxygen during the re-oxidization. Because of not being diluted by air, the fuel reactor outlet stream consists, ideally, of only CO_2 and H_2O, while the air reactor gas releases air with reduced oxygen content. The heat generated in CLC system is equal to that of normal combustion [24]. The stream of CO_2 and H_2O from the fuel reactor can easily be split into CO_2 and water (H_2O) by simple condensation. Thus, an essentially pure CO_2 stream is attained without the need for an expensive and energy consuming gas separation [25,26]. Similar to a normal boiler, the heat generated can be extracted from the air reactor and the two gas streams leaving the air and the fuel reactors to produce steam for e.g., power generation [27]. Additionally, the heat could be used in steam methane reforming, to generate blue hydrogen [22,28].

In a real CLC system, however, complete fuel conversion usually faces several challenges: reaction kinetics, imperfect oxygen carrier-fuel contact and fuel bypassing [29,30]. Therefore, in the case of solid fuels using low-cost oxygen carrier materials, unconverted fuel gases from the fuel reactor can be expected. These gases must be converted to CO_2 and H_2O before downstream operations such as condensation, compression, transportation and storage. To address this, oxy-polishing can be used [29], whereby a pure oxygen stream is introduced to fully oxidize the fuel to CO_2 and H_2O [31,32]. The oxygen for polishing step can be generated from e.g., mature cryogenic technology [31] and the oxygen demand will add only 0.6 % units of energy penalty in the case of 90 % gas conversion a CLC system [27]. Oxy-polishing has been experimentally studied in a 100 kW unit with various fuels and several oxygen carriers [33] at Chalmers University of Technology, and full conversion of fuel reactor gas has been achieved with very low oxygen excess [29]. The oxygen needed in the oxy-polishing unit is basically determined by the oxygen demand in the fuel reactor gas, and also by the gas mixing. In addition to the 100 kW pilot, an oxy-polishing unit was also added to a 1-MW chemical looping pilot at Technical University of Darmstadt, and there are results demonstrating the functionality of the polishing unit [34]. Still, oxy-polishing has not been extensively studied, and optimization to reach full conversion with a minimum of excess oxygen should be performed. Further, the formation of NO_x, should be better understood to optimize the downstream removal of NO_x, which is necessary before transportation and storage of the CO_2.

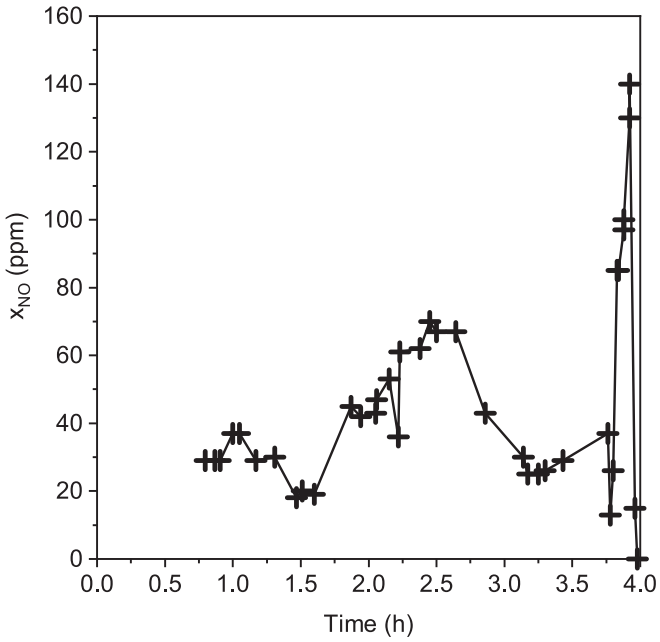

Fig. 2. NO concentration in the gas from the fuel reactor during operation with biomass, i.e. black pellets, and Sinaus manganese ore [37].

The normal paths for NO_x formation, i.e. thermal NO_x, fuel NO_x and prompt NO_x, are closed in CLC for various reasons [35]. In the fuel reactor the only mechanism for NO_x formation is the reaction of nitrogen compounds released from the fuel, e.g., NH_3, with the oxygen carrier. The fate of NO and ammonia (NH_3) was studied in a 300 W gas-fired CLC pilot, by addition of either of these compounds to gas stream introduced to the fuel reactor, i.e. fuel or inert gas [35]. When using ilmenite oxygen carrier, it was found that with a somewhat reduced oxygen carrier, all ammonia was reduced to N_2, and similarly, a somewhat reduced oxygen carrier also completely reduced all NO added to N_2. This was not only seen in presence of fuel, but also in absence of fuel. Nevertheless, significant concentrations of both NO_x and NH_3 are found in the effluent stream from a 100 kW pilot when burning solid fuels like coal in CLC pilots [33], which is likely explained by inadequate contact between gases and oxygen carrier. In contrast, no NO was found in the effluent of a 1 MW CLC plant when using ilmenite when burning coal [36]. If this would also be the case in the full scale, using a fuel reactor with a height of 30–50 m is not known at present.

A literature review on NO_x formation in chemical-looping combustion is given by Lyngfelt et al. [35]. In contrast to coal, no data for high-volatile biomass and NO_x has been published from Chalmers' 100 kW unit. However, NO was actually measured in a previous study. The operational results are published [37], but NO was not included because the analyser was not connected to the data logging. However, the readings of the NO analyser were recorded manually, and the results are shown in Fig. 2 and the average was around 40 ppm, which is much lower than for coal. The data were recorded during 4 h of operation with black biomass pellets and Sinaus manganese ore.

This work studies the formation of gases containing nitrogen in the fuel reactor and their further conversion in the oxy-polishing step. Experiments were carried out in a 100 kW pilot to mimic an upscaled CLC reactor and to get results more relevant to industrial scale. In addition to experiments, a CSTR (continuous stirred-tank reactor) model combining elementary reaction kinetics is employed to find out the mechanism and paths of nitrogen conversion in the oxy-polishing step. Through this work, homogeneous conversion of nitrogen-based gases in the oxy-polishing step is explored, with the aim to support future CLC system design.

Table 1
Physical properties of the Sinaus and ilmenite oxygen carriers.

	Sinaus	Ilmenite
Bulk density (kg·m^{-3})	2090	1900
Median size, d50 (μm)	175	261
Crushing strength (N)	3.5	3.9
Attrition index (wt.%·h^{-1})	1.21	5.7

2. Experiments and simulation

2.1. Oxygen carriers

An ilmenite ore and a manganese ore called Sinaus were the oxygen carriers in the 100 kW experiments. The experiments with Sinaus are from a previous work [16] and some data from NO measurements, not previously published, are used in the current work. Sinaus is a sintered

Table 2
Proximate and ultimate analysis of the solid fuels used in this work.

	Proximate (wt.%, ar)				Ultimate (wt.%, daf)					LHV[b] (MJ/kg)
	FC[a]	V	M	A	C	H	N	S	O[c]	
BP22	13	78	8.5	0.5	53.4	5.5	0.1	0.0	32	18.5
CAL	53.1	29.4	11.0	6.5	78.3	6.6	1.6	0.8	12.7	24.6
BP22-CAL	33	53.7	9.8	3.5	65.9	6.0	0.8	0.4	22.4	21.5

[a] fixed carbon, [b] lower heating value, [c] by difference.

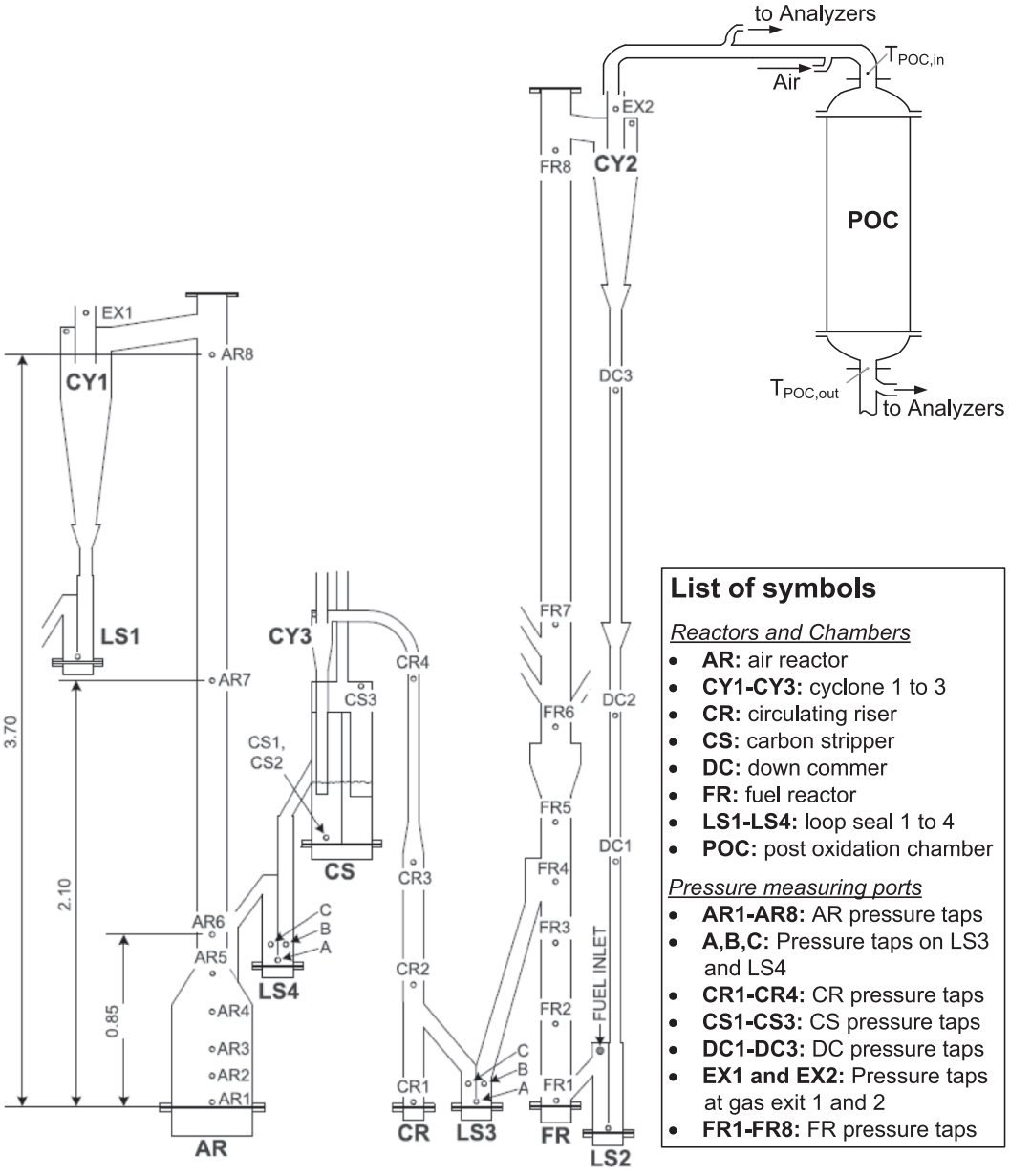

Fig. 3. Sketch of the Chalmers 100 kW pilot and the connected post oxidation chamber, POC.

Table 3
Main operation conditions of the 100 kW pilot.

Test	Oxygen carrier	Fuel	T_{AR} (°C)	T_{FR} (°C)	$T_{POC,in}$ (°C)	P_{th} (kW)	$Q_{air,AR}$ (kg/h)	$V_{air,POC}$ (L_N/min)	Reference
test1	Ilmenite	BP22-CAL	998	949	913	64	155	250	–
test2	Ilmenite	BP22-CAL	1007	956	917	64	155	350	–
test3	Ilmenite	BP22-CAL	1011	959	921	64	155	400	–
test4	Ilmenite	BP22-CAL	1011	957	919	64	155	250	
test5	Ilmenite	BP22-CAL	1009	959	920	64	170	250	–
test6	Ilmenite	BP22-CAL	1008	959	919	64	180	250	–
test7	Ilmenite	BP22-CAL	1009	958	919	64	200	250	–
test8	Ilmenite	BP22-CAL	1011	962	924	76	155	250	–
test9	Sinaus	CAL	1009	968	801	65	130	0	[16]
test10	Sinaus	CAL	1011	972	759	65	155	0	[16]
test11	Sinaus	CAL	1003	971	744	65	175	0	[16]
test12	Sinuas	CAL	998	971	747	65	195	0	[16]
test13	Sinaus	CAL	994	965	768	65	175	100	[16]
test14	Sinaus	CAL	993	963	820	65	175	200	[16]
test15	Sinaus	CAL	995	965	893	65	175	300	[16]
test16	Sinaus	CAL	996	965	953	65	175	400	[16]

Australian manganese ore, where the "Sin" indicates that the material is made from sintered fines and the "aus" indicates the country of origin. The ilmenite is a Norwegian titanium-iron ore which was supplied by Titania A/S and frequently considered as a benchmark oxygen carrier for CLC process [38,39]. Both materials were extensively used in Chalmers' 10 and 100 kW CLC pilots [40] and have shown good reactivity as well as good physical properties [41–43].

The Sinaus manganese ore contains mainly Mn, Fe, Si and Al elements and has a Fe/Mn molar ratio of 0.2, and the ilmenite has 33 % Fe and 25 % Ti [16]. The Sinaus ore was crushed and sieved to particles with a size smaller than 355 μm before use in the 100 kW_{th} unit, while the ilmenite underwent a heat-treatment before use in the unit. The ilmenite was first calcined at 500 °C for 2 h, and then at 950 °C for 12 h. The ilmenite was finally sieved into particles with a median size of d50 = 261 μm and a bulk density of 1900 kg/m^3 before use in the 100 kW unit. Table 1 summarizes some other properties of the two oxygen carriers. The crushing strength of Sinaus and ilmenite was 3.5 N and 3.9 N, respectively. Attrition index of Sinaus and the ilmenite are 1.21 wt%/h and 5.7 wt%/h respectively, according to tests in a jet cup rig [44].

2.2. Solid fuels

A coal named as "CAL" with a mean size of d50 = 130 μm from the Calenturitas mine in Colombia was used in the previous work [16], and the corresponding results are included in the present study. The current work uses a 50/50 mixture of CAL coal and a steam exposed biomass called "black pellets" from Arbaflame in Norway. The "black pellets" were received by our lab in 2022, thus designated as "BP22", and have a mean size of d50 = 1800 μm. The 50/50 mixture of BP22 and CAL is designated as "BP22-CAL". Table 2 displays the proximate and ultimate analysis of the three fuels, determined through ISO and ASTM standard methods. BP22 is a high-volatile biomass fuel, while the CAL coal has significantly lower volatiles. A mixing of BP22 and CAL results in a medium volatiles BP22-CAL fuel and a nitrogen content of 0.8 %, which is significant for the current study. Φ_0, the stoichiometric ratio of moles of O_2 needed to fully burn the fuel per mole carbon, is 1.08, 1.18 and 1.14 for BP22, CAL and BP22-CAL.

2.3. The 100 kW and oxy-polishing unit

Chalmers 100 kW unit was built to contribute to the proof-of-concept of CLC technologies, oxygen carrier testing, design assessment and process optimization. To date, the unit has been used for more than 250 h for CLC tests with over 12 fuels, including coal, petcoke and biomasses, and around 10 oxygen carriers. As seen in Fig. 3, the 100 kW has a high velocity air reactor that drives the circulation and an internally circulating fluidized bed as fuel reactor. The fuel reactor is five meters high and determines the system's height. Between the air and fuel reactor, there is a 4-chamber carbon stripper, which was designed to gasify the residual carbon/fuel from the fuel reactor and returns the gasification products back to the fuel reactor for further conversion. In this way, fuel escaping to the air reactor can be minimized and the carbon capture efficiency can be maximized. In addition, the system has three cyclones and four loop seals, and these together with the fuel reactor, air reactor and carbon stripper are enclosed in a high temperature oven. In the air reactor, the oxidation of the oxygen carrier is exothermic, thus the reactor's temperature can sometimes rise rapidly. To avoid overheating the air reactor, an air-cooling jacket is installed surrounding the lower part of the air reactor and this can be used to control the reactor temperature.

A post oxidation chamber (POC) for oxy-polishing is installed downstream of the fuel reactor cyclone. In this way, combustibles remaining in the gas from the fuel reactor can be sent directly to the POC for further conversion. The POC is a cylindrical tube, vertically situated in the system and has a diameter of 0.30 m and a height of 1.50 m. The POC doesn't have external heating devices, so it was insulated with ceramic blankets to maintain the reactor's temperature. Two K-type thermal couples were used to measure the temperatures at the POC inlet and outlet. For safety reasons, instead of using pure O_2, the current work used air as oxidant in the POC. Any real-world application would of course use oxygen to avoid the dilution with N_2. The air flow entering the POC was split into two tangential streams to enhance the mixing of air and combustibles.

2.4. Experimental procedure

Experimental data are mainly from a new campaign with ilmenite as the oxygen carrier and BP22-CAL as the fuel (test1-test8), as well as a previous campaign using Sinaus and CAL (test9-test16) [16], both at a similar operation temperature of around 950–970 °C in the fuel reactor. The POC inlet temperature is in the range of 747–924 °C and is lower than the fuel-reactor temperature, because of heat loss from the gas path before the POC inlet. The air reactor was normally kept at around 1000 °C. The gas flow at the fuel reactor inlet is kept at 10 kg/h and at the air reactor inlet is 130–200 kg/h, and the corresponding gas velocities at the operational temperatures are 0.92 m/s at the fuel reactor inlet and 1–1.54 m/s at the air reactor inlet. Given the terminal gas velocities (u_t) are 0.91 m/s for particles in the fuel reactor and 0.83 m/s in the air reactor, the two reactors are both in fast fluidization regime. Furthermore, the velocity in the thinner riser of the air reactor increases by a factor of around six, whereas the velocity in the fuel reactor could increase by more than ten times depending on the fuel conversion. The operational conditions are summarized in Table 3. Based on these data the effect of key operational parameters, e.g., POC air flow, oxygen

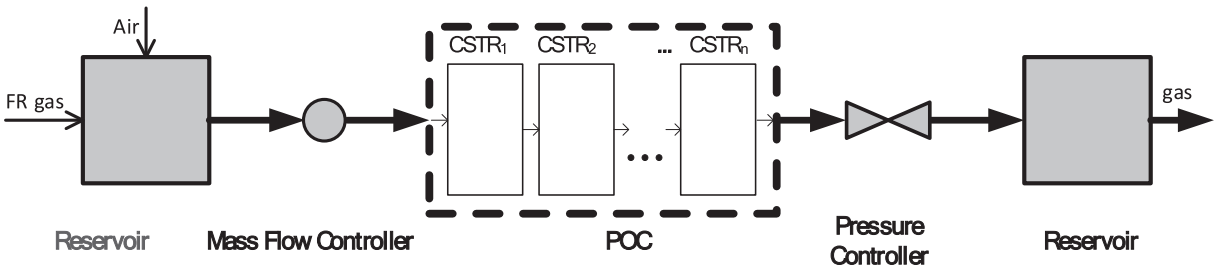

Fig. 4. Schematic of the POC reactor model with a chain of CSTRs and associated gas and pressure controllers.

Table 4
Initial temperature (°C), average dry gas concentration (% for CO, CH_4, H_2, CO_2 and N_2, ppm for NO), oxygen demand (Ω_{OD}, %) and wet gas flows F_i (mol/s) at the POC model's inlet.

$T_{POC,in}$	$x_{CO,FR}$	$x_{CH4,FR}$	$x_{H2,FR}$	$x_{CO2,FR}$	$x_{NO,FR}$	$x_{N2,FR}$	Ω_{OD}	
916	6.5	3.3	7.1	54.8	397	28.2	18.3	
F_{O2}	F_{N2}	F_{CO}	F_{CH4}	F_{H2}	F_{CO2}	F_{NO}	F_{H2O}	F_{NH3}
0	4×10^{-2}	9.33×10^{-3}	4.67×10^{-3}	1×10^{-2}	7.77×10^{-2}	5.7×10^{-5}	0.57	3.1×10^{-4}

carrier-fuel pair, fuel power and air reactor flow, which also controls the solids circulation rate [45], can be evaluated. Steam is used to fluidize the fuel reactor, loop seals and carbon stripper, while N_2 is added to the fuel container, to sweep the fuel conveying path, and to the pressure measuring ports to avoid blocking. Sampling gas from the fuel reactor, air reactor and POC is extracted and cooled down to remove water vapor, before being sent to gas analyzers for concentration measurement. Concentrations of CH_4, CO, CO_2, H_2 and O_2 of the fuel reactor and POC were measured with Rosemount™ NGA2000 gas analyzers. The air-reactor gas was subject to measurements of CO, CO_2 and O_2 concentrations with a SIDOR Sick Maihak analyzer. NO and NO_2 concentrations were measured with Rosemount™ X-Stream gas analyzers. All the concentration data were logged with a rate of 1 HZ and collected with a computer. Condensates from the fuel reactor and POC were collected and sent to SGS Analytics Sweden AB for analysis of NO_2^-, NO_3^- and NH_4^+.

2.5. POC model with the elementary reaction kinetics

Homogeneous gas-phase reactions in the POC were simulated with a reactor model and elementary kinetics parameters proposed in a GRI-Mech 3.0 package [46], which includes 325 reactions and 53 species, covering all the reactions considered to be relevant for the POC. The kinetics were incorporated in the open-source tool Cantera [47], which is coupled with Python codes to form a zero-dimensional model, e.g. a continuous stirred-tank reactor (CSTR), for the simulation. A chain of CSTRs with an identical volume was used to simulate a plug-flow reactor that was used to model the POC. As seen in Fig. 4, the model has an upstream reservoir to mimic the gas supply, and a mass flow controller to regulate the gas flow. The POC consisted of a number of CSTRs, a pressure controller to regulate the gas pressure and a downstream reservoir which was used as an exhaust gas sink. Various numbers of CSTRs can be used in the model, but based on comparison with experiments and previous work [29] three CSTRs were selected to predict the POC performance, so the volume of each CSTR is 0.036 m^3 which is one third of the POC volume (0.11 m^3). The average of the fuel reactor gas flows and temperatures from tests 1, 2 and 3 in Table 3 were selected as inputs to the model. Average values of the input data are presented in Table 4. The model can calculate gas composition and temperature at the exit of each CSTR. As mentioned before, the model can simulate more than three hundred reactions, but this work mainly focuses on general combustion reactions and nitrogen reactions. Further, important reaction paths are obtained through the model, and these can be used to track the conversion of different gas components and be of potential use in future system design.

3. Data processing

3.1. Gas flows and oxygen demand

The total gas flow rate F_i (mol/s) of component i (i=CH_4, CO_2, CO, H_2 or O_2) at the fuel reactor exit was calculated using the gas concentrations x_i and the total molecular flow (F_{out}, mol/s) of gases leaving the fuel reactor. The equation below was used for the calculation.

$$F_i = x_i \bullet F_{out} \tag{1}$$

where F_{out} was obtained through a method based on nitrogen balance, i.e. assuming the total molecular flow of nitrogen (F_{N2}, mol/s) at the entry and exit of the fuel reactor is identical.

$$F_{out} = \frac{F_{N_2}}{1 - \sum x_i} \tag{2}$$

A dimensionless parameter called oxygen demand, Ω_{OD}, is used to understand the desired ratio of oxygen for complete oxidation of the unconverted fuel-reactor gases (CO, CH_4 and H_2) over the stoichiometric oxygen needed for the solid fuel's full combustion which is calculated via Φ_0 as shown in section 2.2 above and the denominator in equation (3) below. The oxygen demand for the fuel reactor is obtained through equation (3).

$$\Omega_{OD} = \frac{0.5x_{CO} + 2x_{CH_4} + 0.5x_{H_2}}{\Phi_0(x_{CO} + x_{CH_4} + x_{CO_2})} \tag{3}$$

3.2. Normalized gas concentrations

In order to compare the results from different operational conditions, the gas concentrations at fuel reactor exit $(x_i)_{FR}$ and POC exit $(x_i)_{POC}$ are normalized by comparison with the total carbon concentration of each reactor, i.e. $(x_{CH4} + x_{CO} + x_{CO2})_{FR}$ and $(x_{CH4} + x_{CO} + x_{CO2})_{POC}$. The normalized concentration is denoted as $x_{i,N,j}$ (j = FR for the fuel reactor and POC for the POC reactor) and calculated through equation (4).

$$x_{i,N,j} = \frac{x_{i,j}}{(x_{CH_4} + x_{CO} + x_{CO_2})_j} \tag{4}$$

For NO, $x_{i,N,j}$ is multiplied by 10^6 which gives the concentration in ppm/100 %CO_2, to indicate the concentration in the undiluted CO_2 stream.

3.3. Sum of contaminants

The O_2, CO, H_2, CH_4 and NO from the oxy-polishing unit are considered as contaminants for CO_2 compression, transportation and sequestration. To compare with the required concentrations for piping and transportation, these gases are normalized to dry-and-nitrogen free

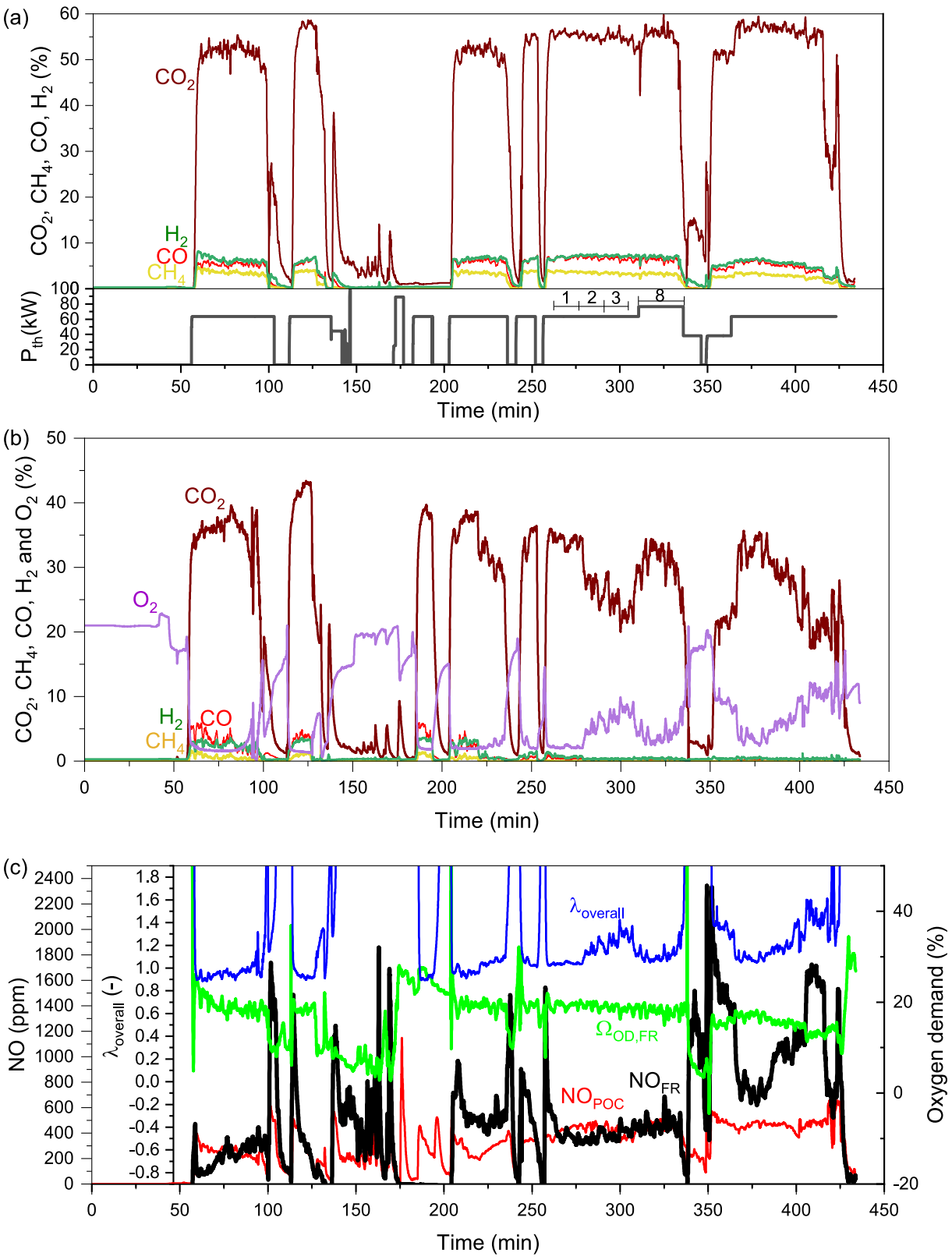

Fig. 5. (a) measured fuel reactor gas (CO_2, CO, CH_4, H_2) concentration and fuel thermal power, numbers 1–3, 8 refer to tests shown in Table 3, (b) measured CO_2, CO, CH_4, H_2 and O_2 concentration at the POC exit and (c) measured NO concentrations at the FR and POC exits, fuel reactor oxygen demand ($\Omega_{OD,FR}$), and the overall oxygen ratio ($\lambda_{overall}$).

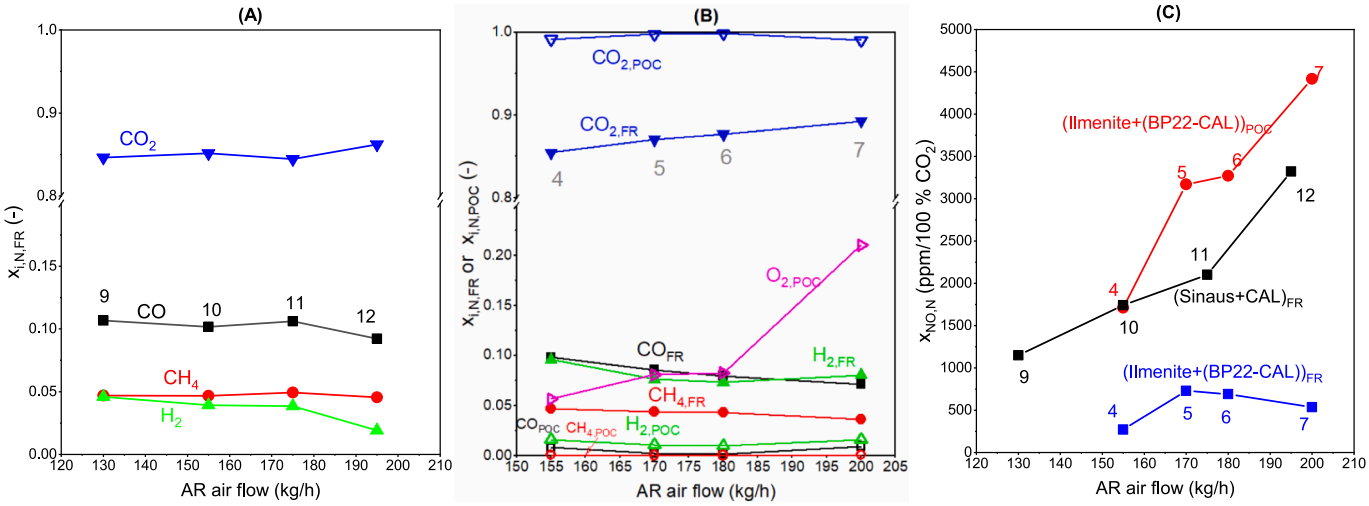

Fig. 6. (a) effect of air reactor flow on the normalized concentrations of CO_2, CO, CH_4 and H_2 in the fuel reactor when using the pair "Sinaus + CAL" and when the POC air flow was zero, (b) effect of air reactor flow on the normalized concentrations of CO_2, CO, CH_4, H_2 and O_2 in the fuel reactor (marked with the subscript "FR") and POC (marked with the subscript "POC") when using "Ilmenite+(BP22-CAL)" and POC air flow was 250 LN/min, and (c) effect of air reactor flow on the normalized NO concentration at the exit of the fuel reactor (marked with the subscript "FR") and POC (marked with the subscript "POC"). Numbers in the graphs show the test numbers from Table 3.

(DNF) concentrations through the equation (5.1) below and the sum of the DNF concentrations (SUM_{DNF}) in equation (5.2) is used to optimize the POC performance. The nitrogen removed is mainly from pressure taps and from pressurizing the fuel feed, i.e. nitrogen that would not be present in a real-world application.

$$x_{i,DNF} = \frac{x_{i,POC}}{(1 - x_{H_2O} - x_{N_2})_{POC}} \tag{5.1}$$

$$SUM_{DNF} = \sum x_{i,DNF} \tag{5.2}$$

3.4. Overall oxygen ratio

The overall oxygen ratio, $\lambda_{overall}$, evaluates the total available oxygen (from oxygen carrier and POC air) over the stoichiometric oxygen needed for full combustion, see equation (6). It can be obtained with the modified oxygen demand, Ω_{OD^*}, which also includes the oxygen present after the POC, cf. eq. (3).

$$\lambda_{overall} = 1 - \Omega_{OD^*} = 1 - \frac{0.5x_{CO} + 2x_{CH_4} + 0.5x_{H_2} - x_{O_2}}{\Phi_0 (x_{CO} + x_{CH_4} + x_{CO_2})} \tag{6}$$

4. Results and Discussions

4.1. Reaction progress

Fig. 5 displays the fuel power, actual gas concentrations at the exit of both the POC chamber and fuel reactor, and the nitrogen monoxide concentration together with oxygen demand and the overall oxygen ratio for operation with ilmenite and BP22-CAL. Drops in gas concentrations and fuel power are a result of fuel stops that were needed for various reasons, e.g. to add more fuel to the fuel bin or to clean sampling gas lines. The outlet of fuel reactor has mainly 50–60 % CO_2 and 5–10 % of CH_4, CO and H_2 (Fig. 5a), but the latter were further oxidized in the oxy-polishing step with air in the POC (Fig. 5b). When the oxygen ratio ($\lambda_{overall}$) exceeded 1.03 at around 260 min, complete oxidation was achieved, albeit with some excess of oxygen. The POC concentration of all the gases is lower than that in the fuel reactor as a result of dilution by the POC air. When the POC air flow is raised, see tests 1, 2 and 3, the overall oxygen ratio obviously rises, leading to higher excess of oxygen and a more complete combustion in POC. When the fuel power was increased from 64 kW (test 1) to 76 kW (test 8), the fuel reactor had a slight increase in the CO_2 concentration. But the CO_2 in POC for test 1 and test 8 are very close, again as a result of dilution by the large air flow. The NO concentration at the fuel reactor exit is around 300–500 ppm, and in some cases even around 1000 ppm, which is in some cases (e.g., between 205 and 235 min) higher than the NO in POC and in other cases (e.g., 260–280 min) lower than the POC values, as seen in Fig. 5c. The oxygen demand is about 10–20 % which is typical of this pilot and lower than what is reached with only biomass.

4.2. Effect of air reactor flow

Fig. 6 shows the effect of air reactor flow on the gas concentrations in the fuel reactor and POC when using "Sinaus + CAL" and "Ilmenite+(BP22-CAL)". A raised air flow to the air reactor leads to more CO_2, and less CO, CH_4 and H_2 leaving the fuel reactor, because of increased oxygen carrier circulation leading to a more oxidized state of the oxygen carrier, cf. Fig. 6 a and b. Because of better combustion in the fuel reactor, there are less combustibles entering the POC, which may explain the slight decreases in the H_2 and CO concentration noted at the POC exit when the air reactor gas flow is higher, except the test 7 where a slight increase is seen in Fig. 6b. The influence of combustibles is complex as will be shown in the modelling section below. Thus, less combustibles entering the POC may reduce the temperature increase in the POC and, as a consequence, lower the gas conversion.

Fig. 6c shows that more NO is generated in the POC at a higher air reactor air flow. This is not unexpected, when conversion improves in the fuel reactor, the air ratio will increase in the POC when the addition of air is constant. In addition, Fig. 6c compares the normalized NO concentration between fuel reactor and POC with the ilmenite oxygen carrier and BP22 + CAL as fuel. As seen, the NO increases quite significantly in the POC and this might be attributed to further oxidation of NH_3 in the POC. Moreover, it can be seen that NO is significantly lower for "Ilmenite+(BP22-CAL)" than for "Sinaus + CAL". This can be explained by ilmenite giving lower NO than manganese ore, which was found in another study, albeit with another manganese ore [35]. But, as seen from Fig. 2, black pellets are expected to give very low NO, so this is likely the main factor explaining the lower concentration of NO.

4.3. Effect of POC air flow

Addition of air to POC provides oxygen for combustion of the

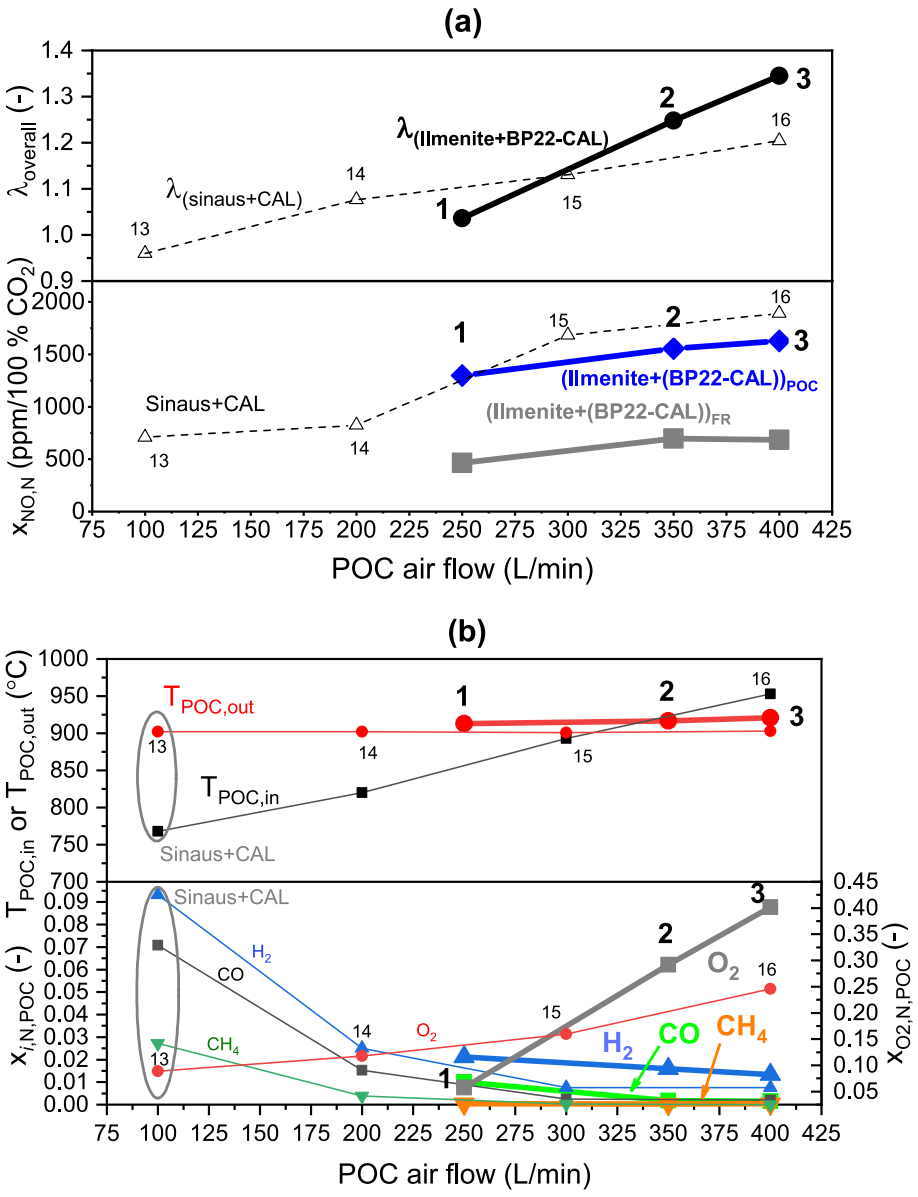

Fig. 7. Effect of POC air flow (a) on the normalized NO concentration at fuel reactor and POC outlet and the overall oxygen ratio and (b) on the temperature at POC inlet ($T_{POC,in}$) and outlet ($T_{POC,in}$) and normalized gas concentration (CH_4, CO, H_2 and O_2). Thicker lines show the data with "Ilmenite+(BP22-CAL)" with air reactor flow of 155 kg/h, and the thinner- dashed lines show the data with "Sinaus + CAL" with air reactor flow of 175 kg/h, the numbers show the test number from Table 3.

unconverted CH_4, CO and H_2 that come from the fuel reactor. The overall oxygen ratio increases almost linearly with air addition to the POC, as seen in Fig. 7a. The lowest overall oxygen ratio is at around $\lambda_{overall} = 0.96$ when the air flow was 100 L/min, while the highest is $\lambda_{overall} = 1.35$ when the air flow was 400 L/min. With an increased oxygen ratio, the normalized NO concentration also increases, and this again is attributed to the oxidation of NH_3 in presence of oxygen. The highest NO concentration was $X_{NO,N} = 1500$ ppm/100 $\%CO_2$ at $\lambda_{overall} = 1.35$ for Ilmenite+(BP22-CAL), and 1800 ppm/100 $\%CO_2$ at $\lambda_{overall} = 1.2$ for Sinaus + CAL. The normalized gas concentrations and POC temperatures are presented in Fig. 7b. The Sinaus + CAL and the Ilmenite+(BP22-CAL) pairs show similar behavior in combustion and temperature at the POC out. Complete oxidation for both cases can be achieved with high POC flows (more than 250 L/min) for both coal or a BP22-CAL. The excess of O_2 is high and is higher for the BP22-CAL as compared to the Sinaus + CAL. The increase in O_2 versus POC air flow is less steep for "Sinaus + CAL", which is explained by elutriated char burning in the POC, as observed in previous work [29]. When the elutriated char is high as in the case with coal (CAL), part of the O_2 in the POC air is used for char conversion, lowering the excess oxygen observed. Thus, as the air addition to the POC increases, the rise in O_2 excess is less for CAL. In the case of BP22-CAL, on the other hand, the char content is low (33 %) leading to lower char elutriation and less oxygen is needed to convert the elutriated char. Thus, the O_2 increase with BP22-CAL is faster than with CAL.

It is also clear that for BP22-CAL the measured and normalized H_2 is around 0.01–0.02 and is not converted even at very high air excess. It is reasonable to assume that this is an artifact and probably caused by the difficulties of measuring H_2 on-line because of the interference with other gases, even though the H_2 analyzer has a compensation for important other gases like CO_2 and CH_4.

4.4. Nitrogen in the condensates

The condensate collected from the gas sampling streams from test 5 and test 6 was analyzed. Nitrogen species found in the condensate are

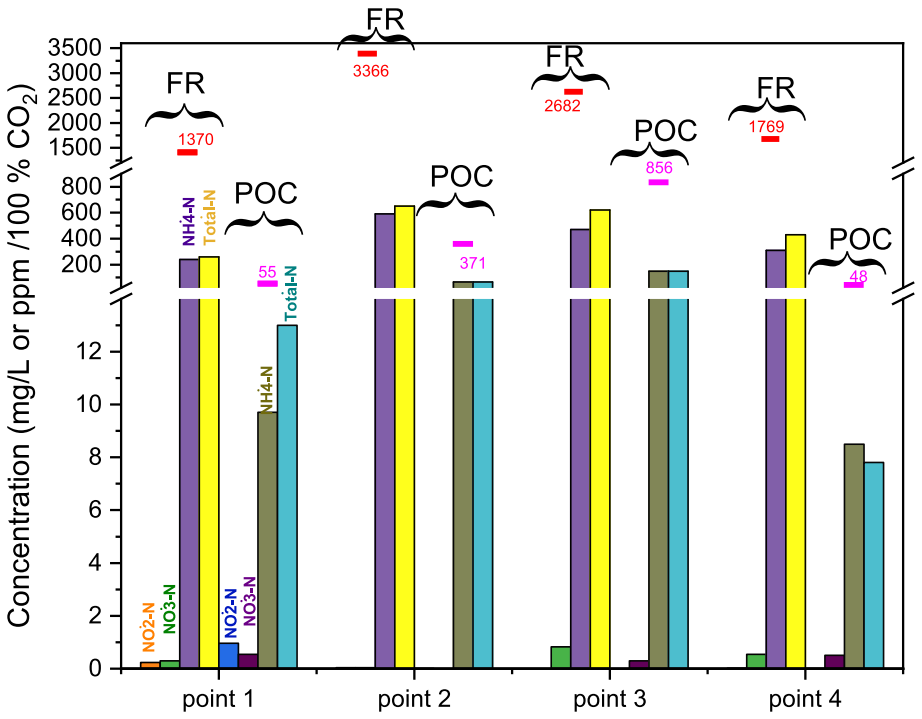

Fig. 8. Comparison of nitrogen distribution in the fuel reactor and POC condensates, point 1 and point 2 are from test 5, and point 3 and point 4 are from test 6. Bars show condensate concentrations (mg/L), whereas numbers shown together with dash lines are the actual normalized concentrations of NH_3 (ppm/100%CO_2).

NO_2^-, NO_3^- and NH_4^+, but only the ammonium ion (NH_4^+) was found in any significant concentration, see Fig. 8. The data indicates high concentrations of NH_3 in the gas from the fuel reactor and that part of the NH_3 was not fully converted in the POC. The concentrations of NH_3 are significantly reduced in the POC, 4–35 times in the four tests shown. From a material balance, the concentrations can be estimated, 1300 – 3400 ppm/100 %CO_2 after the fuel reactor and 40– 800 ppm/100 %CO_2 after the POC. Thus, the NH_3 after the fuel reactor is several times higher than the 400–700 ppm/100 %CO_2 of NO, see Figs. 5-6. The ratio is higher than in a previous mass balance of N in the 100 kW unit with coal, where the concentration of NH_3 was a little more than twice as high as that of NO [33]. The higher ratio for coal + biomass is not surprising as a higher release of NH_3 is typical of biomass volatiles.

A comparison to the increase in NO in Fig. 6c and Fig. 7 indicates that a majority of the NH_3 in the gas is oxidized to NO. Thus, the low concentrations of NO from biomass, cf. Fig. 2 can be very significantly increased in the oxy-polishing step. If all the fuel nitrogen were converted to NO it would give 10–11 thousand ppm/100 %CO_2. Thus, it is

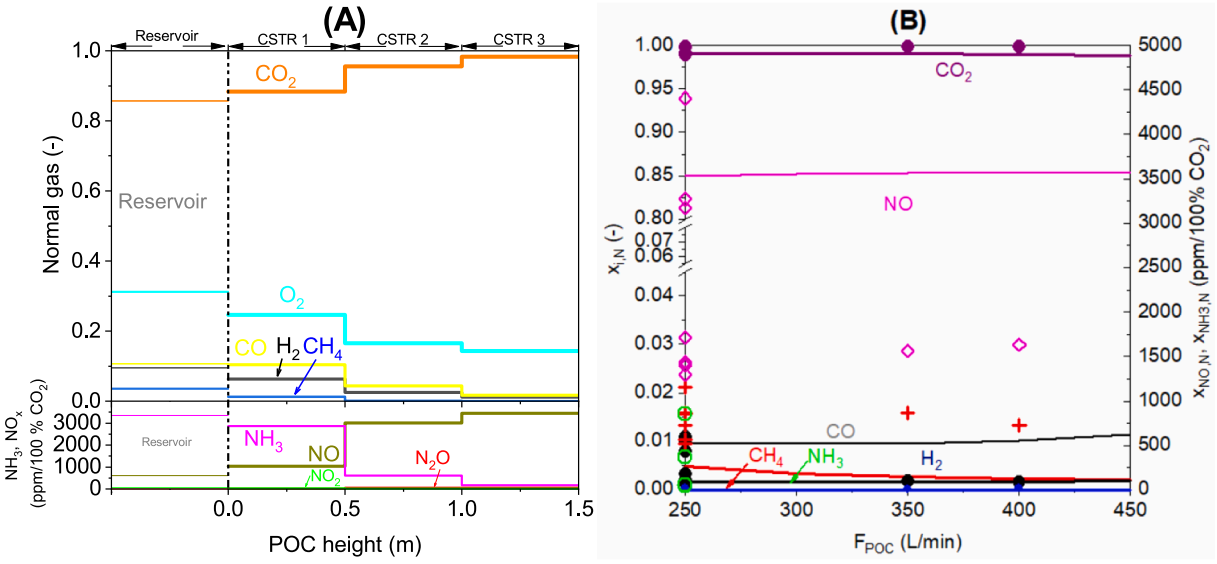

Fig. 9. (a) gas concentration profiles of the upstream reservoir (left of the vertical dash line) and POC (right of the vertical dash line) after simulation with three chained CSTRs, (b) comparison between model (lines, e.g. H_2(-), NH_3(-), CO(-), CH_4(-)) and experiments (symbols in same colours as the lines, e.g. H_2(+), NH_3(X), CO(●), CH_4(●)).

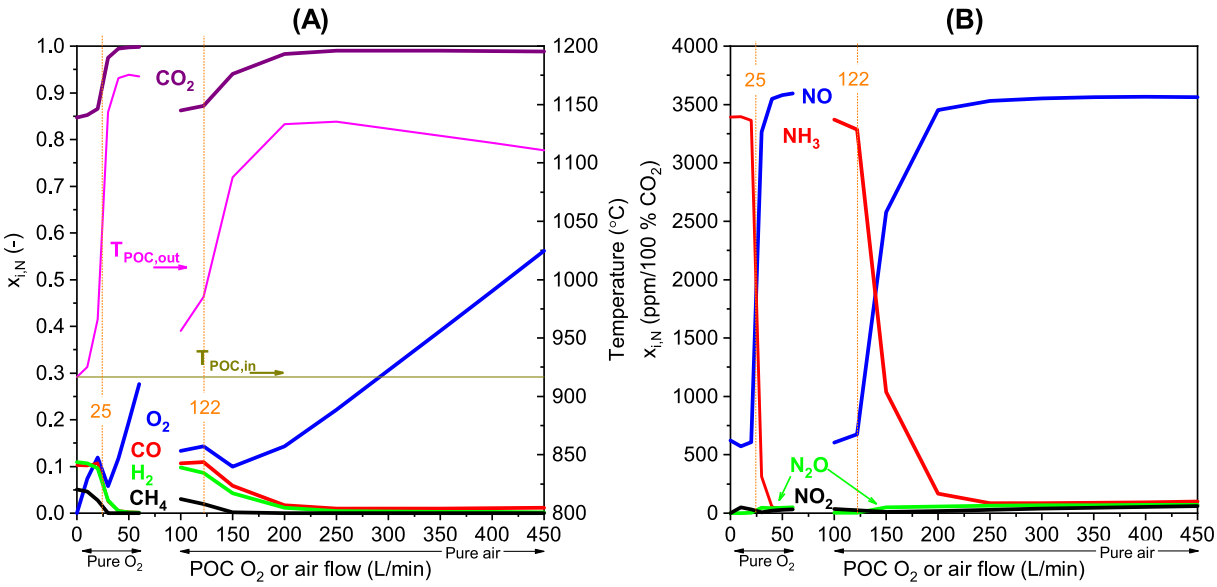

Fig. 10. Effect of POC flows on (a) normalized CO, CH_4, H_2, O_2, CO_2 concentrations and the POC out temperature, CO is hidden behind the H_2 line in the case with pure O_2, and (b) the nitrogen gases with either pure O_2 or air as the oxidation gas. Vertical dashed lines are the stoichiometric flows.

clear that a majority of the fuel nitrogen is converted to N_2 in the fuel reactor.

4.5. Conditions at the inlet of the modelled POC reactor

As mentioned in section 2.5, we used the average of the POC inlet temperature and the fuel-reactor gas flows from tests 1, 2 and 3 as input data, *c.f.* Table 3. Table 4 below shows these average values. The flow of NH_3 was estimated with the NH_4^+ concentration in the fuel-reactor condensate, as discussed in section 4.4 above, and the flows of other gases were calculated with the measured gas concentration and the total gas flows at fuel reactor exit.

4.6. Modelling results

4.6.1. Validation of the POC model

In the 100 kW unit, we used air as oxidant in the oxy-polishing step. But in a real oxy-polishing unit, pure O_2 should be used. To explore oxy-polishing performance, we set up a reactor model based on elemental kinetics to simulate the reactions in POC. Fig. 9a presents the gases in the reservoir, the model's results along the POC height, and Fig. 9b compares the model and experimental results. As seen in Fig. 9a, the model shows the combustion of combustibles along the POC, with CO_2 increasing and combustibles decreasing. The concentration in each CSTR is constant because of the assumption of perfect mixing. Fig. 9b shows that the model predicts well the concentrations of CO_2, and CH_4 from available experimental data. However, the model overestimates H_2 conversion and underestimates CO conversion to some extent. The

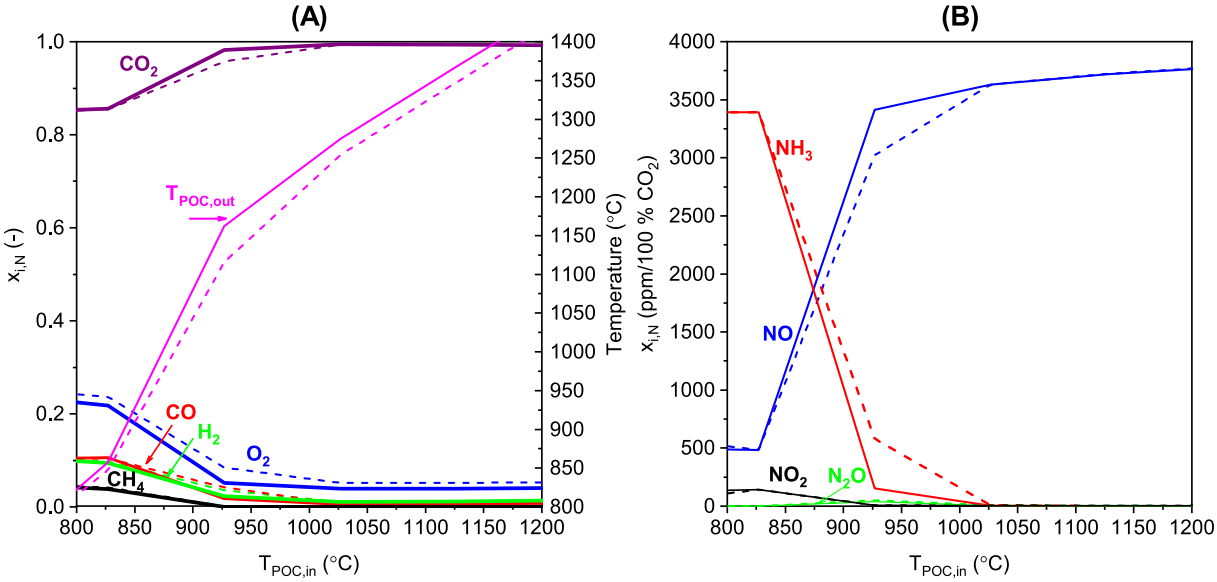

Fig. 11. Effect of poc inlet temperature on (a) normalized ch_4, CO, H_2, O_2, CO_2 concentrations and the POC out temperature ($T_{POC,out}$), and (b) the nitrogen gas concentrations. The oxidation gas in the POC is either 150 L/min air (dashed lines) or 30 L/min O_2 (solid lines). Some gases (e.g., H_2, NO_2 and N_2O) have almost the same concentration when using air and pure O_2.

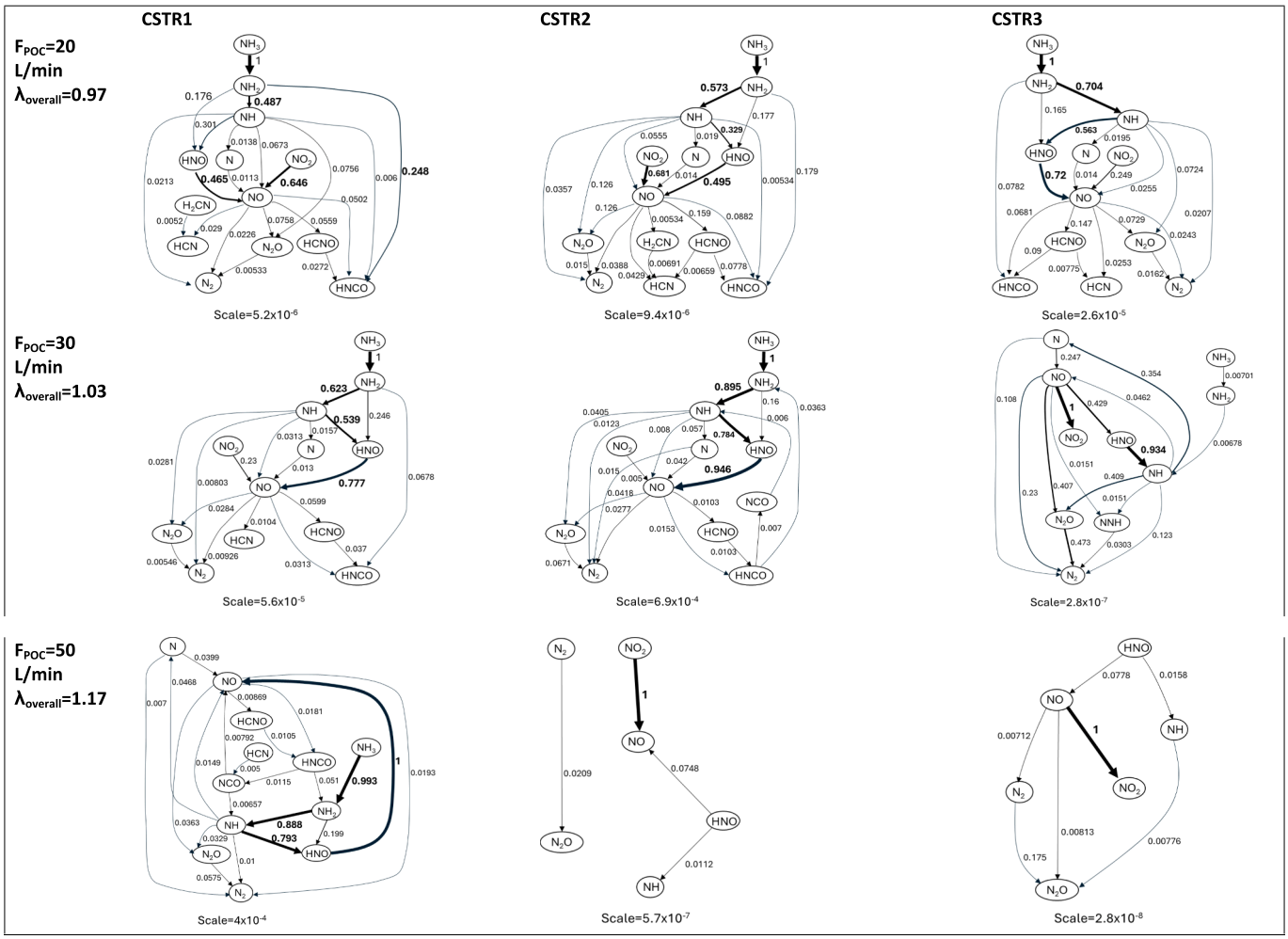

Fig. 12. Reaction paths of N-based species in CSTR1, CSTR2 and CSTR3 in sub-stoichiometric (20 L/min O_2), slightly over-stoichiometric (30 L/min O_2) and highly over-stoichiometric (50 L/min O_2) conditions, with averaged data from the 100 kW ilmenite+(BP22-CAL) experimental results as input. The POC inlet temperature was 916 °C. The values together with the arrows are dimensionless which were normalized against the maximum net element flux that takes a unit of kmol/m^3/s [48] and the scaling factor of the normalization were provided below each, for example 0.175 × 2.8e-08 gives the net flux for the direct N_2 conversion to N_2O in the case of F_{POC} = 50 L/min and CSTR3.

incomplete conversion of H_2, however, could be an artifact, as discussed in Section 4.3. The model also overestimates the NO concentration, and this might be because of the uncertainty in the estimated incoming NH_3 concentration, which was derived from NH_4^+ concentration in the condensate. Overall, the model predicts the experimental data well.

4.6.2. Comparison between the use of pure O_2 and air in the POC

Fig. 10 compares the change of gas concentration and POC outlet temperature when using either pure O_2 (0–60 L/min) or air (100–450 L/min) in the POC. Increased flows lead to less combustibles in both cases, and complete/near-complete gas conversion can be reached when the flows are significantly higher than the stochiometric flows, which are 25 L/min for pure O_2 and 122 L/min for air. As the gas flow increases, the O_2 concentration shows a decrease immediately after the stoichiometric point, which could be explained by the strong temperature increase around the stoichiometric point. At higher flows the temperature at the POC exit starts to decrease as it is cooled by the added gas. Conversion of NH_3 to NO and of the combustibles to CO_2 and H_2O is high when the POC flow is over the stoichiometric value. Since the temperature is much lower than what is needed for thermal NO_x (usually more than 1500 °C) the N_2 in air does not react with the gases. The major difference between the use of O_2 or air lies in; i) a faster increase in temperature and a higher peak POC temperature for O_2. ii) a final CO_2 concentration slightly lower than 1 for air, while complete combustion can be reached with oxygen. Better conversion with oxygen is expected because of higher temperature and residence time.

Fig. 11 displays the effect of POC inlet temperature on the gas concentrations. When the temperature is lower than 825 °C, the fuel has a very low conversion, and the CH_4, CO, H_2 and NH_3 flow is almost the same as that in the fuel reactor. Above 825 °C, conversion of combustibles increases with temperature and a major part of the combustibles is converted at 925 °C while complete combustion is reached at temperatures higher than 1000 °C. At the lower inlet temperatures, the NH_3 conversion is low but there is also formation of NO_2 and N_2O, but at higher temperatures there is only NO. This NO corresponds to a third of the fuel-N. Again, as the temperature is lower than that needed for thermal NO_x formation, the N_2 in the air added to the POC is not involved in the formation of NO.

4.6.3. Reaction path with pure oxygen

The Python code for the POC model can be used to extract the reaction paths in all the three CSTRs which make up the POC reactor in the model. With this feature, the model can extract all relevant reactions and their reaction rates when given an element of interest. When putting these reactions together, the dominant reactions can be confirmed and thus the reaction paths for certain components can be identified. Fig. 12

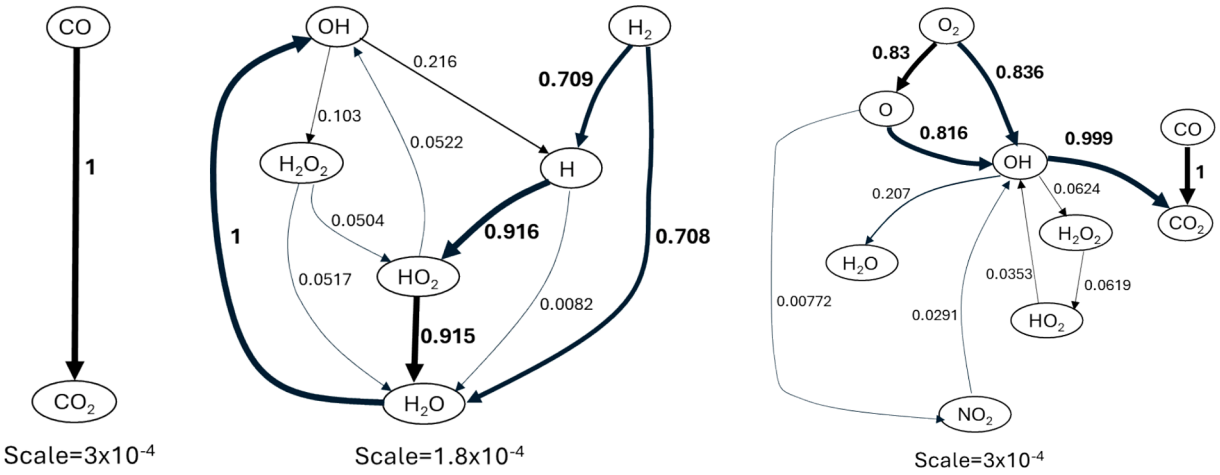

Fig. 13. Reaction paths of C, H and O related compounds in CSTR3 of the POC model with 50 L/min O_2 at 916 °C.

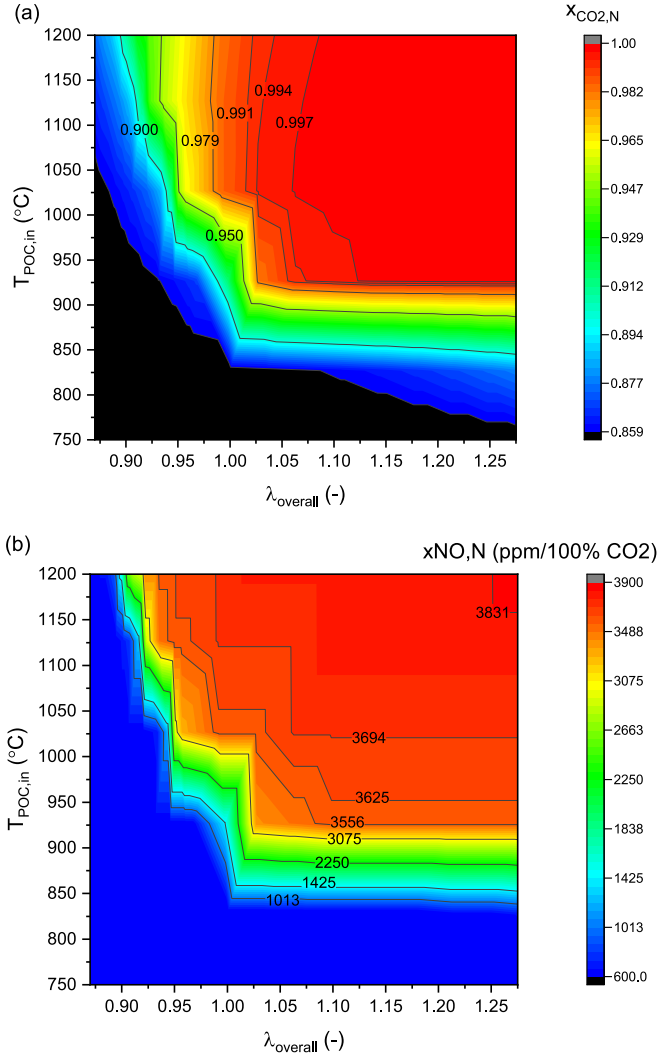

Fig. 14. Modelled results for (a) CO_2 concentration, (b) NO concentration using oxygen and the current POC design, i.e., a diameter of 0.3 m and a length of 1.5 m.

below presents the N-based reaction paths for the three CSTRs when using a sub-stoichiometric flow (20 L/min O_2), a slightly over-stoichiometric flow (30 L/min O_2) and a highly over-stoichiometric flow (50 L/min O_2). The early CSTRs (e.g., CSTR1 and CSTR2) have more complex reactions than the later CSTRs, while the later reactor reactions have a higher intensity. In the case of 20 L/min O_2, the CSTR2 has a reaction rate of 1.8 times that in CSTR1, and the reaction in the third CSTR is 50 times faster than in the first CSTR. This phenomenon could be an effect of temperature increase which is around a 60 °C increment when comparing CSTR3 and CSTR1 in this specific case. In the case of 30 L/min O_2 and 50 L/min O_2, the later CSTRs have simpler final products and fewer intermediate reactions before generating the final products. In the CSTR1 and CSTR2, HCNO, HNCO and HNO are usually the intermediates while in the last reactor (CSTR3) the conversion is more straightforward. The higher POC flows clearly lead to less complexity of reactions in each CSTR. When the POC flow is sub-stoichiometric, the available oxygen is not enough for complete oxidation, leading to more side reactions and intermediate reactions being involved.

Fig. 13 below shows reaction paths of CO, H_2, O_2 conversion in the CSTR3 of the POC model with O_2 flow of 50 L/min. Here, the oxygen is over-stoichiometric for all the reactions and no side products are found. Therefore, the conversion of CO to CO_2 is straightforward in the CSTR3, while the conversion of H_2 and O_2 involves some intermediate reactions.

4.6.4. *Mapping the operational region with pure oxygen*

This section maps the operational region with pure oxygen (O_2) that would be useful for oxy-polishing scaleup in commercial CLC system. Inlet temperature and oxygen excess (or overall oxygen ratio) are key parameters for fuel conversion in the POC. Their effects are presented with contours curves in Fig. 14. A normalized CO_2 concentration higher than 0.997 is reached when the temperature is higher than 925 °C and the overall oxygen ratio is higher than 1.07. Under these conditions the conversion of NH_3 to NO is also very high, as seen in Fig. 14b. On the contrary, when the temperature is lower than 825 °C it is very difficult to convert the fuel components even at a high oxygen ratio and it is not possible to reach high conversion if inlet temperature is below 925 °C.

The sum of dry-and-nitrogen-free concentrations of O_2, CO, H_2, CH_4 and NO, i.e. SUM_{DNF}, as calculated through equation 5, is used as an indicator to find an optimal condition where the sum of residual combustibles, NO and unused O_2 is the least. Below this sum will be referred to as contaminants. To fulfil CO_2 purity criteria for transport and storage, the contaminants will need to be removed by e.g. distillation and therefore it makes sense to minimize the sum of these. Note that N_2 formed coming from e.g. fuel-N is not included among these, which can be motivated by no, or at least much less stringent, limits for N_2. Fig. 15 shows the sum of contaminants at different POC inlet temperatures versus overall oxygen ratio. The sum goes through a minimum as the overall oxygen ratio increases, and thus the optimal oxygen ratio can be

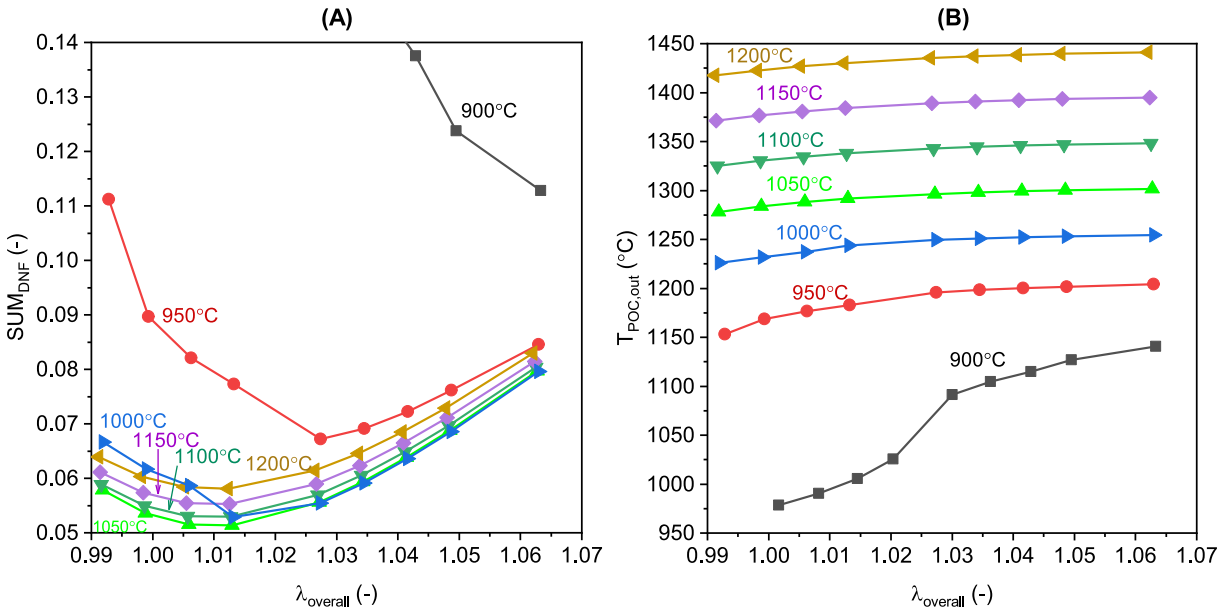

Fig. 15. (a) SUM_{DNF}, *c.f.* equation 5, sum of the O_2, CO, H_2, CH_4, and NO dry-and-nitrogen-free concentration and (b) POC outlet temperature when varying the overall oxygen ratio at different temperatures. All with the 100 kW's current POC design which has a diameter of 0.3 m and a length of 1.5 m.

Table 5
Fuel-reactor wet gas concentrations (% or ppm) used in the model in the cases of F0.5, F1 and F2, the total wet gas flow (F_{total}, mol/s) and oxygen demand (Ω_{OD}) for the three cases.

Cases	$x_{CO,FR}$	$x_{CH4,FR}$	$x_{H2,FR}$	$x_{CO2,FR}$	$x_{NO,FR}$ [a]	$x_{N2,FR}$	$x_{NH3,FR}$ [a]	$x_{H2O,FR}$	F_{total}	Ω_{OD}
F0.5	0.67	0.33	0.71	11.1	81	5.7	220	81.5	0.701	9.8
F1 [b]	1.3	0.65	1.4	10.8	79	5.6	440	80.1	0.713	18.3
F2	2.5	1.27	2.71	10.5	77	5.4	840	77.4	0.737	31.5

[a] with a unit of ppm, [b] these are wet concentrations and thus different to those in table 4.

found depending on temperature. There is a strong effect of inlet temperature, and when it is increased from 950 to 1050 °C, the sum is greatly reduced. But above 1050 °C, the sum starts to rise and consequently, the sum of contaminants reaches the lowest values at an inlet temperature of 1050 °C. Normally, fuel reactors in pilots have operated at temperatures of 950–970 °C or less, with the exception of an 80 kW pilot that has been operated with biomass and a fuel reactor exit temperature above 1050 °C [49]. At 950 °C, an optimal conversion is attained at an overall oxygen ratio of 1.03, and the sum of dry-and-nitrogen free O_2, CO, H_2, CH_4 and NO is 0.0672, corresponding to a CO_2 purity of 93.3 %.

Below, the impact of the amount of combustibles coming from the fuel reactor under different overall oxygen ratios is presented. The amount of combustibles (CH_4, CO, H_2 and NH_3) is varied by multiplying the flows of CH_4, CO, H_2 and NH_3 with factors of 0.5 and 2, represented as F0.5 and F2 in Table 5 below, with the original concentration denoted as F1. In addition to wet concentrations of CO, CH_4, H_2, CO_2, NO, N_2, NH_3, H_2O, Table 5 shows the total wet gas flow leaving the fuel reactor and the fuel reactor's oxygen demand.

Results are presented in Fig. 16 and are shown for three different inlet temperatures and for two POC diameters 0.3 and 0.5 m (D0.3 and D0.5), to indicate the effect of residence time. The diagrams clearly illustrate that a low amount of combustibles can give a higher sum of contaminants and how this is related to the temperature increase in the POC. Thus, in case of the smaller diameter (D0.3) with a residence time in the order of 1 s, the highest amount of combustibles (F2) gives the lowest sum of combustibles, except for the highest inlet temperature of 1050 °C. For the larger diameter (D0.5), corresponding a residence time in the order of 3 s, the results are more mixed. Thus, the highest amount of combustibles (F2) gives the lowest sum of contaminants at 850 °C, the middle amount of combustibles, F1, gives best results for 950 °C, while the lowest amount of combustibles gives the least contaminants at 1050 °C. In conclusion, a sufficient temperature needs to be reached in the POC to give high conversion. The results suggest that a sufficient POC outlet temperature is 1250 °C for the shorter residence time and around 1150 °C for the longer residence time. Fig. 16 also shows that in all cases the longer residence time, D0.5, gives a significant reduction of the contaminants at the minimum point, except for 850 °C and F0.5.

4.6.5. *Effect of the POC size with pure oxygen*

Fig. 17 displays the effect of POC volume and gas residence time on the sum of contaminants (SUM_{DNF}) and the temperature at the POC exit ($T_{POC,out}$) with a POC inlet temperature of 950 °C and 1050 °C. The gas residence time is seen on the secondary X-axis of Fig. 17 and as expected, the gas conversion and temperature increase with a longer residence time. In the 100-kW's current design, the POC has a volume of 0.11 m^3 and a gas residence time of around 1 s, as seen with the vertical-dashed line labelled with current design in the figure. In an upscaled CLC system, a reasonable residence time in oxy-polishing unit could be 3 s. Increasing the diameter of the current design to 0.5 m results in a residence time of 3 s, see the line labelled with Design I in the figure. The Design I lowers the contaminants to 3.37 %, which is a good improvement as compared to the 7.73 % reached with the current design. Further increase of the POC size, Design II, results in additional reduction of contaminants to 2.22 %. However, Design II, with a residence time of around 14.2 s would be unrealistic in a commercial application. When the POC inlet temperature is increased from 950 °C to 1050 °C, the temperature at the POC outlet shows a similar increase. The effect of the higher temperature is considerable when the gas residence time is shorter than 2 s. Beyond this, the amount of contaminants with the two

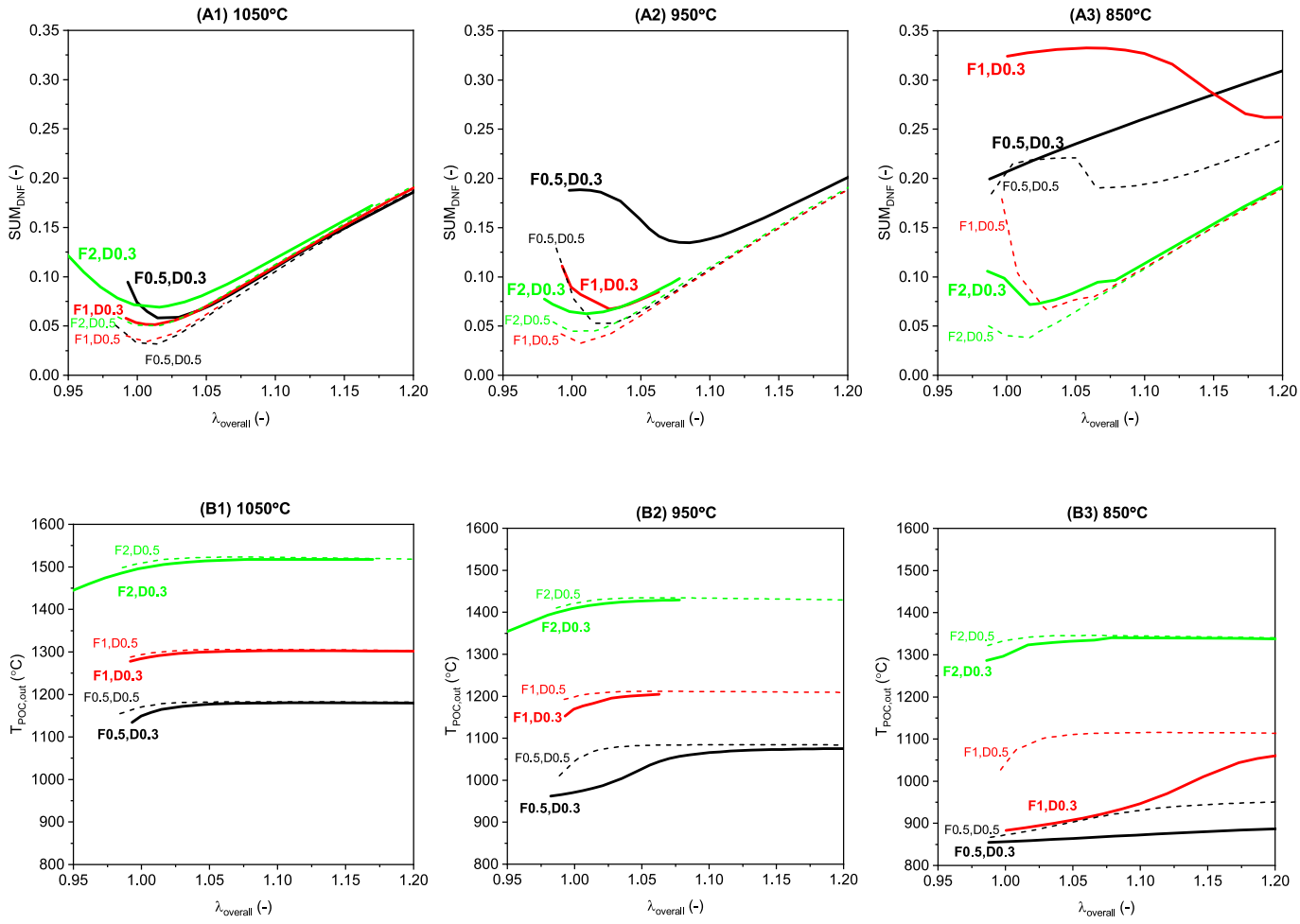

Fig. 16. (A) sum of the dry-and-nitrogen-free concentration of O_2, CO, H_2, CH_4, and NO and (B) POC outlet temperature versus overall oxygen ratio at different inlet temperatures. FxDy refers to amount of combustibles multiplied by a factor *x* (0.5, 1 or 2) and POC diameter *y* (0.3 or 0.5 m). D0.3 is presented with thick-solid lines and the D0.5 is presented with thin-dashed lines.

inlet temperatures is quite similar.

4.7. Discussion

4.7.1. Thermal NO_x

The formation of NO from nitrogen and oxygen in air is commonly known as thermal NO_x. The reaction is strongly temperature dependent and "a frequently applied rule-of-thumb is to ignore the thermal formation of NO at temperatures below about 1800 K", [50], i.e. around 1500C. In normal combustion the maximum temperature possible is given by the adiabatic flame temperature, which is typically around 2000 °C for common fuels. Even if furnaces are cooled, it is difficult to avoid high temperatures in flames and associated formation of thermal NO_x. In chemical-looping combustion, there are no flames, neither in the fuel reactor, nor in the air reactor and temperatures are below 1100 °C so there is no risk of thermal NO_x formation in the chemical-looping process.

However, this does not necessarily apply to the post-oxidation chamber, which is expected to be adiabatic. This also means that, assuming full conversion, the adiabatic flame temperature is reached. As noted in Fig. 15 temperatures of up to 1500 °C are possible if the oxygen demand would be very high. Moreover, the residence time in the adiabatic POC would be a few seconds in contrast to the normally very short gas residence time at high temperature in flames.

The kinetics of thermal NO formation is well known and the formation of NO in moles/(cm^3•s) is given by [51].

$$\frac{d}{dt}[NO] = \frac{6\times10^{16}}{T^{1/2}} exp\left\{\frac{-69,090}{T}\right\} \times [N_2] \times [O_2]^{1/2} \quad (7)$$

where T is the absolute temperature and [NO], [N_2] and [O_2] is the concentration of NO, N_2 and O_2 in moles/cm^3. In Table 6 the formation of NO, in ppm/s, is given versus temperature for different concentrations of O_2 and N_2. It is evident that significant amounts of NO would form in air at 1500 °C with a residence time of a few seconds, i.e., in contrast to the normally very short gas residence time in flame zones.

However, in the case of the POC the concentrations of O_2 and N_2 are low and formation of thermal NO should be well below the ppm level even at the highest temperatures, cf. Table 6.

4.7.2. CO_2 purification and optimal oxygen addition

For normal chemical-looping combustion, i.e. in contrast with CLOU where oxygen carriers releasing gas phase oxygen [52], unconverted combustibles are likely impossible to avoid. Thus, purification is needed, and it is also clear that the purification is greatly facilitated if oxygen is added, whereby oxygen and combustibles form CO_2 and H_2O, thus increasing the purity of CO_2. Further, the amount of addition of O_2 is a matter of optimization, and here it is assumed that the optimum is when the amount of contaminants are at minimum, which occurs at a slight excess of oxygen.

To find the POC optimal conditions where the contaminants are minimized, simulations were made by varying the oxygen flow for the current design, Design I and II. The concentrations of the various

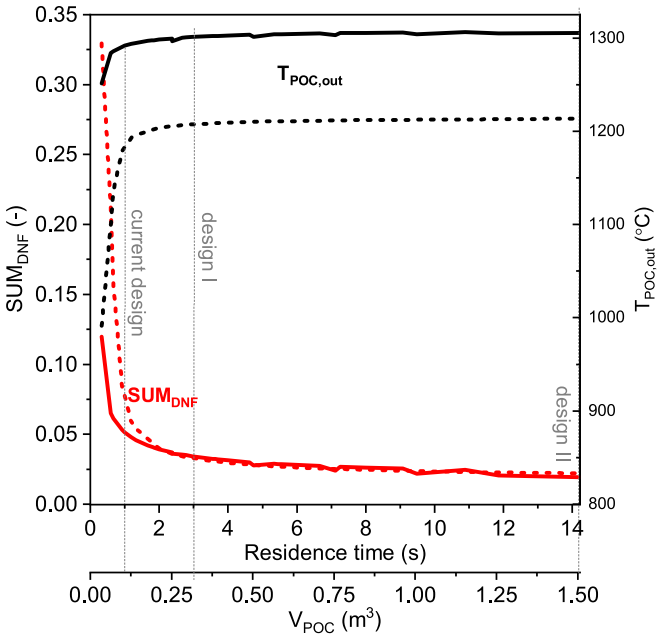

Fig. 17. Effect of POC volume (V_{POC}) and the corresponding gas residence time on the sum of contaminants (SUM_{DNF}, red lines) and POC outlet temperature ($T_{POC,out}$, black lines). The POC inlet temperature was set to 950 °C (dashed lines) and 1050 °C (solid lines) and the O_2 flow was fixed to 28 L/min. Vertical-dashed lines present three different POC designs (current design, design I and design II). (For interpretation of the references to colour in this figure legend, the reader is referred to the web version of this article.)

Table 6
Formation of NO versus temperature, ppm/s for different percentages of O_2/N_2.

T, °C	Air	Design I at optimum
O_2/N_2, %	21/79	1.5/0.7
1200	0.007	0.00002
1300	0.13	0.0003
1400	1.7	0.004
1500	16	0.04

contaminants are shown in Table 7 together with a comparison to an example of limits set for transportation and storage. The sums of contaminants for the three designs are 6.72 %, 3.27 % and 1.74 %. Thus, for Design I the fraction of contaminants, not including N_2, is reduced from 23.6 % to 3.3 %, clearly emphasizing the importance of oxy-polishing step for the purification.

NO is only 10 % of the contaminants for the design with around 3 s residence time, so this is not likely to make a large difference for the later purification. But, as was discussed in the introduction there is great uncertainty regarding the expected concentrations of NO and NH_3 in the outlet of a full-scale fuel reactor, as they could potentially be very low. Moreover, biomass often has low nitrogen content. The BP22 used in this study only contained 0.1 % N, which, if converted to N_2, is only around 800 ppm if normalized. On the other hand, the Calenturitas coal would give around 9000 ppm of N_2.

As seen in Table 7, the concentration of contaminants is around 3.3 % for the case with a reasonable residence time, Design I. From the examination of the effect of inlet gas concentrations and inlet temperatures in Fig. 16, it appears difficult to reach significantly below this level. Here, the concentration of oxygen contrasts most with the required level, i.e. around 15,000 ppm compared to < 10 ppm. After oxygen comes NO with around 3400 ppm compared to < 10 ppm. On the other hand, the combustibles have significantly lower ratios between actual and required concentrations, i.e. H_2 10,300 versus < 50 ppm and

Table 7
Comparison between the required purity for CO_2 piping and transportation and the normalized concentrations achieved at the minimum of contaminants at 950 °C with the 100 kW's POC current reactor and two larger designs (Design I and Design II).

	Required [53]	**Current design ID 0.3, L1.5**	**Design I ID 0.5, L1.5**	**Design II ID 0.8, L3.0**
Optimal condition		*O_2 flow 30 L/min $\lambda_{overall}$ 1.037 tr 1.1 s T_{POCout} 1196 °C*	*O_2 flow 27 L/min $\lambda_{overall}$ 1.007 tr 2.7 s T_{POCout} 1204 °C*	*O_2 flow 26 L/min $\lambda_{overall}$ 0.9996 tr 13.2 s T_{POCout} 1209 °C*
Component	ppm	ppm	ppm	ppm
H_2O	≤30	–	–	–
O_2	≤10	40,900	14,500	4400
SO_x	≤10	–	–	–
NO_x	≤10	3300 (only NO)	3400 (only NO)	3400 (only NO)
H_2S	≤9	–	–	
CO	≤100	8600	4500	2800
CH_4	–	0	0	0
Amine	≤10	–	–	–
Ammonia, NH_3	≤10	0	0	0
Hydrogen, H_2	≤50	14,300	10,300	6900
Formaldehyde	≤20	–	–	–
Acetaldehyde	≤20	–	–	–
Mercury	≤0.03	–	–	–
SUM_{DNF} (O_2, NO_x, CO, CH_4 and H_2)		6.72 %	3.27 %	1.74 %

CO 4500 versus < 100 ppm.

When the downstream purification of the gas is designed, there are different options [53]. One would be to have a sufficiently extensive distillation to reach ppm levels. However, since NO is likely to be a lot lower than in this optimization, another option could be to remove the oxygen by catalytic combustion, which would significantly lower the demands on the distillation. In that case, the optimal oxygen addition would also be higher, leading to a lowering of combustible gases like H_2 and CO, thus reducing the need for extensive distillation further.

A species not included in the contaminants discussed so far, is the nitrogen that is formed from the fuel nitrogen. With a biofuel, this could be low as noted above. But, N_2, as well as argon, could also enter as a contaminant in the oxygen for oxy-polishing or by air ingress. The purity of the oxygen used in the POC is a matter of optimization. Air ingress is normal in boilers, firstly because flue gas channels are at under-pressure to assure flue gases are not released in the boiler house, and secondly because inleakage is not a significant problem. But in the case of a CO_2 stream that needs purification any oxygen or nitrogen that leaks in is associated with added costs, which would motivate measures to assure that air ingress is eliminated, or at least reduced to low levels.

Maximum N_2 is not always specified, but when it is, it is < 2.4 to < 4 % [54]. Similarly, the maximum CH_4, when specified, is 1–4 %. In some cases, the maximum N_2 is limited by a CO_2 purity requirement, e.g. > 99 % purity [53].

Ideally, the POC is a perfect plug-flow reactor with the gases entering being perfectly mixed. The model, however, assumes perfect mixing in the three CSTR stages, which will give lower conversion than an ideal plug-flow reactor, and the three stages was selected to match the experimental results and to account for imperfect mixing. Nonetheless, it is very important that the oxygen addition in a large-scale unit is done in a way that provides good mixing.

Normally, when discussing the performance of the CLC process, it is assumed that the oxygen demand should be minimized. However, as seen in Fig. 16, a low oxygen demand will not give the temperature increase needed in the POC to attain good conversion. Consequently, it

appears as if the oxygen demand has an optimum level, and, if it falls below this level, measures to increase the oxygen demand or extra fuel addition to the POC could be needed.

The model results suggest that a rather high oxygen demand is needed to reach sufficient temperature. However, the needed oxygen demand is overestimated because of the high flows of N_2 and steam that are added for fluidization, pressure taps and fuel feeding in the 100 kW unit, cf. Table 4. A heat balance using the additional steam flows expected in a full-scale application, here assumed to be 1/6 of the gas flow in the fuel reactor, indicates that an oxygen demand of around 8 % would be sufficient to give a 250 °C temperature increase, e.g. from 950 to 1200 °C similar to the cases in Table 7.

5. Conclusions

The oxy-polishing process was studied in a 100 kW CLC pilot and simulated with a zero-dimensional reactor model integrated with elementary reaction kinetics. Fuel-nitrogen conversion and reaction paths are closely focused. Below are the conclusions that can be drawn from the current work.

i. Fuel nitrogen is mostly converted to N_2 in the fuel reactor, but a large amount of NH_3 and some NO is also formed. Most of the NH_3 is oxidized to NO in the oxy-polishing step, resulting in dramatic increase in NO.
ii. Oxygen in the air added reacts with the combustibles, and the conversion of these depend on temperature, oxygen excess, amount of combustibles and residence time.
iii. An oxy-polishing reactor model with three one-dimensional stages is validated with the 100 kW experimental results and can be used for future up-scaling of the design.
iv. Reaction intermediates have been identified through the reactor model. The intermediates are more relevant in sub-stoichiometric conditions and the first part of the POC reactor.
v. Based on the model, the oxy-polishing can reach an optimal oxidation with an overall oxygen ratio of 1.037 and a content of contaminants of 6.7 %, for a residence time around 1.1 s. Increasing the residence time to 2.7 s, the optimal overall oxygen ratio is 1.007 and the amount of contaminants to 3.3 %. A further increase in residence time to 13.2 s lowered the amount of contaminants to 1.7 %.
vi. The model also highlights the necessity to reach sufficient temperature in the POC, which is dependent on the inlet temperature and the amount of combustibles in the gas coming from the fuel reactor. Thus, to achieve good conversion, the POC temperature likely needs to reach around 1150 °C for a residence time of 3 s. This would mean that it could be a problem if the oxygen demand is too low, which would then require either addition of supporting fuel to the POC or operational measures to increase the oxygen demand.
vii. For a fuel reactor temperature of 950 °C, the oxygen demand should be around 8 % to safely reach the needed temperature increase in the POC.

CRediT authorship contribution statement

Daofeng Mei: Writing – review & editing, Writing – original draft, Visualization, Methodology, Investigation, Formal analysis, Data curation, Conceptualization. **Anders Lyngfelt:** Writing – review & editing, Supervision, Resources, Project administration, Methodology, Investigation, Funding acquisition, Data curation, Conceptualization. **Tobias Mattisson:** Writing – review & editing, Supervision, Project administration, Funding acquisition. **Carl Linderholm:** Writing – review & editing, Resources, Project administration, Investigation.

Declaration of competing interest

The authors declare the following financial interests/personal relationships which may be considered as potential competing interests: Daofeng Mei reports administrative support was provided by Huazhong Agricultural University. If there are other authors, they declare that they have no known competing financial interests or personal relationships that could have appeared to influence the work reported in this paper.

Acknowledgement

This work was supported by the Swedish Research Council, project Nitrogen Chemistry in Chemical-Looping Combustion and Oxygen-Carrier Aided Combustion (2016-05487) and the Swedish Energy Agency, as part of the projects OxyCar-FBC, conducted within the framework of ERA-NET Bioenergy, (P43936-1) and the project Kemcyklisk förbränning av biomassa och avfall (51585-1).

Support Information

The Python codes used in this work and related files can be found and downloaded through the link below.

https://drive.google.com/drive/folders/1SvFFjbFRPLInkeagGXLjqjt845yKWBCb?usp=sharing.

A tutorial on how to use the codes can be found through my YouTube channel.

https://youtu.be/h1fgKZZEj7A?si=m5p2e7TC6-qP_z9d

Data availability

Data will be made available on request.

References

[1] D. Gielen, F. Boshell, D. Saygin, M.D. Bazilian, N. Wagner, R. Gorini, The role of renewable energy in the global energy transformation, Energy Strateg. Rev. 24 (2019) 38–50, https://doi.org/10.1016/j.esr.2019.01.006.
[2] L.M.P. Caballero, F.N. D'Angelo, R. Tschentscher, A. Gottschalk, A.M. Salem, D. Carbonell, M. Dudita-Kauffeld, A. Bruch, E. Alamaro, L. Pasquini, P. Ceroni, A. Grozdanova, S. Privitera, B. Vermang, P. Schulz, D. Mencarelli, L. Pierantoni, M. Midrio, W. Leithead, I. Gurruchaga, R. Haberl, J. Vermaut, M. Kauffeld, Developing the next generation of renewable energy technologies: an overview of low-TRL EU-funded research projects, Open Res. Europe 3 (2023), https://doi.org/10.12688/openreseurope.15276.12682.
[3] A. Lyngfelt, M. Fridahl, S. Haszeldine, FinanceForFuture: Enforcing a CO_2 emitter liability using atmospheric CO_2 removal deposits (ACORDs) to finance future negative emissions, Res. Soc. Sci. 107 (2024) 103356, https://doi.org/10.1016/j.erss.2023.103356.
[4] A. Lyngfelt, B. Leckner, T. Mattisson, A fluidized-bed combustion process with inherent CO_2 separation: application of chemical-looping combustion, Chem. Eng. Sci. 56 (2001) 3101–3113, https://doi.org/10.1016/S0009-2509(01)00007-0.
[5] M.E. Boot-Handford, J.C. Abanades, E.J. Anthony, M.J. Blunt, S. Brandani, N. Mac Dowell, J.R. Fernandez, M.-C. Ferrari, R. Gross, J.P. Hallett, R.S. Haszeldine, P. Heptonstall, A. Lyngfelt, Z. Makuch, E. Mangano, R.T.J. Porter, M. Pourkashanian, G.T. Rochelle, N. Shah, J.G. Yao, P.S. Fennell, Carbon capture and storage update, Energy Environ. Sci. 7 (2014) 130–189, https://doi.org/10.1039/C3EE42350F.
[6] W.K. Lewis, E.R. Gilliland, Production of pure carbon dioxide, US Patent 2,665,971, 1954.
[7] M. Ishida, D. Zheng, T. Akehata, Evaluation of a chemical-looping-combustion power-generation system by graphic exergy analysis, Energy 12 (1987) 147–154, https://doi.org/10.1016/0360-5442(87)90119-8.
[8] A. Lyngfelt, A New Combustion Technology, Greenhouse Gas Issues No. 73 (2004) 2-3.
[9] A. Lyngfelt, H. Thunman, Chapter 36 - Construction and 100 h of Operational Experience of A 10-kW Chemical-Looping Combustor, in: D.C. Thomas (Ed.), Carbon Dioxide Capture for Storage in Deep Geologic Formations, Elsevier Science, Amsterdam, 2005, pp. 625-645. https://www.entek.chalmers.se/lyngfelt/co2/PrototypePaperChapter36.PDF.
[10] J. Adánez, A. Abad, Chemical-looping combustion: Status and research needs, Proc. Combust. Inst. 37 (2019) 4303–4317, https://doi.org/10.1016/j.proci.2018.09.002.
[11] Y. Liu, K. Yin, J. Wu, D. Mei, J. Konttinen, T. Joronen, Z. Hu, C. He, Ash chemistry in chemical looping process for biomass valorization: A review, Chem. Eng. J. 478 (2023) 147429, https://doi.org/10.1016/j.cej.2023.147429.

[12] A. Lyngfelt, Chemical Looping Combustion: Status and Development Challenges, Energy Fuels 34 (2020) 9077–9093, https://doi.org/10.1021/acs.energyfuels.0c01454.
[13] X. Wang, Y. Gong, D. Shao, D. Chen, Experimental investigation and structural optimization prediction of a novel carbon stripper for solid-fuel chemical looping combustion, Chem. Eng. J. 470 (2023) 143955, https://doi.org/10.1016/j.cej.2023.143955.
[14] N. Berguerand, A. Lyngfelt, Design and operation of a 10kW$_{th}$ chemical-looping combustor for solid fuels – Testing with South African coal, Fuel 87 (2008) 2713–2726, https://doi.org/10.1016/j.fuel.2008.03.008.
[15] L. Shen, J. Wu, J. Xiao, Q. Song, R. Xiao, Chemical-Looping Combustion of Biomass in a 10 kW$_{th}$ Reactor with Iron Oxide As an Oxygen Carrier, Energy Fuels 23 (2009) 2498–2505, https://doi.org/10.1021/ef900033n.
[16] C. Linderholm, M. Schmitz, M. Biermann, M. Hanning, A. Lyngfelt, Chemical-looping combustion of solid fuel in a 100kW unit using sintered manganese ore as oxygen carrier, Int. J. Greenhouse Gas Control 65 (2017) 170–181, https://doi.org/10.1016/j.ijggc.2017.07.017.
[17] Xinhuanet, The world's largest 4MW$_{th}$ chemical looping combustion demonstration unit was built at Dongfang Boiler (translated from Chinese). http://www.xinhuanet.com/energy/20230328/c372659fad5444f4b42d5d72b784716a/c.html (accessed September 23, 2024).
[18] Z. Li, The dynamic system research team has made significant progress in the research of chemical looping combustion technology (translated from Chinese). Web page. Release time March 27. https://www.te.tsinghua.edu.cn/info/1095/3291.htm (accessed December 29, 2024).
[19] Deliverable D6.4: 3MW$_{th}$ CLC demonstration unit testing, https://cheers-clc.eu/wp-content/uploads/2024/07/D6.4-3MWth-CLC-demonstration-unit-testing-2.pdf (accessed December 29, 2024).
[20] T. Song, L. Shen, Review of reactor for chemical looping combustion of solid fuels, Int. J. Greenhouse Gas Control 76 (2018) 92–110, https://doi.org/10.1016/j.ijggc.2018.06.004.
[21] J. Adanez, A. Abad, F. Garcia-Labiano, P. Gayan, L.F. de Diego, Progress in Chemical-Looping Combustion and Reforming technologies, Prog. Energy Combust. Sci. 38 (2012) 215–282, https://doi.org/10.1016/j.pecs.2011.09.001.
[22] A. Lyngfelt, D. Pallarès, C. Linderholm, F. Lind, H. Thunman, B. Leckner, Achieving Adequate Circulation in Chemical Looping Combustion—Design Proposal for a 200 MW$_{th}$ Chemical Looping Combustion Circulating Fluidized Bed Boiler, Energy Fuels 36 (2022) 9588–9615, https://doi.org/10.1021/acs.energyfuels.1c03615.
[23] S. Daneshmand-Jahromi, M.H. Sedghkerdar, N. Mahinpey, A review of chemical looping combustion technology: Fundamentals, and development of natural, industrial waste, and synthetic oxygen carriers, Fuel 341 (2023) 127626, https://doi.org/10.1016/j.fuel.2023.127626.
[24] E. Jerndal, T. Mattisson, A. Lyngfelt, Thermal analysis of chemical-looping combustion, Chem. Eng. Res. Des. 84 (2006) 795–806, https://doi.org/10.1205/cherd05020.
[25] J. Fan, L. Zhu, H. Hong, Q. Jiang, H. Jin, A thermodynamic and environmental performance of in-situ gasification of chemical looping combustion for power generation using ilmenite with different coals and comparison with other coal-driven power technologies for CO_2 capture, Energy 119 (2017) 1171–1180, https://doi.org/10.1016/j.energy.2016.11.072.
[26] S. Mukherjee, P. Kumar, A. Yang, P. Fennell, Energy and exergy analysis of chemical looping combustion technology and comparison with pre-combustion and oxy-fuel combustion technologies for CO_2 capture, J. Environ. Chem. Eng. 3 (2015) 2104–2114, https://doi.org/10.1016/j.jece:2015.07.018.
[27] A. Lyngfelt, B. Leckner, A 1000 MW$_{th}$ boiler for chemical-looping combustion of solid fuels – Discussion of design and costs, Appl. Energy 157 (2015) 475–487, https://doi.org/10.1016/j.apenergy.2015.04.057.
[28] T. Pröll, A. Lyngfelt, Steam Methane Reforming with Chemical-Looping Combustion: Scaling of Fluidized-Bed-Heated Reformer Tubes, Energy Fuels 36 (2022) 9502–9512, https://doi.org/10.1021/acs.energyfuels.2c01086.
[29] D. Mei, C. Linderholm, A. Lyngfelt, Performance of an oxy-polishing step in the 100 kW$_{th}$ chemical looping combustion prototype, Chem. Eng. J. 409 (2021) 128202, https://doi.org/10.1016/j.cej.2020.128202.
[30] D. Mei, A.H. Soleimanisalim, A. Lyngfelt, H. Leion, C. Linderholm, T. Mattisson, Modelling of gas conversion with an analytical reactor model for biomass chemical looping combustion (bio-CLC) of solid fuels, Chem. Eng. J.433 (2022) 133563, https://doi.org/10.1016/j.cej.2021.133563. Part 2.
[31] A.R. Smith, J. Klosek, A review of air separation technologies and their integration with energy conversion processes, Fuel Process. Technol. 70 (2001) 115–134, https://doi.org/10.1016/S0378-3820(01)00131-X.
[32] C. Zheng, Z. Liu, Oxy-fuel combustion: fundamentals, theory and practice, Academic Press, Elsevier, 2017 https://www.sciencedirect.com/book/9780128121450/oxy-fuel-combustion.
[33] C. Linderholm, P. Knutsson, M. Schmitz, P. Markström, A. Lyngfelt, Material balances of carbon, sulfur, nitrogen and ilmenite in a 100kW CLC reactor system, Int. J. Greenhouse Gas Control 27 (2014) 188–202, https://doi.org/10.1016/j.ijggc.2014.05.001.
[34] J. Ströhle, M. Orth, B. Epple, Design and operation of a 1MW$_{th}$ chemical looping plant, Appl. Energy 113 (2014) 1490–1495, https://doi.org/10.1016/j.apenergy.2013.09.008.
[35] A. Lyngfelt, A. Hedayati, E. Augustsson, Fate of NO and Ammonia in Chemical Looping Combustion—Investigation in a 300 W Chemical Looping Combustion Reactor System, Energy Fuels 36 (2022) 9628–9647, https://doi.org/10.1021/acs.energyfuels.2c00750.
[36] P. Ohlemüller, J. Ströhle, B. Epple, Chemical looping combustion of hard coal and torrefied biomass in a 1MW$_{th}$ pilot plant, Int. J. Greenhouse Gas Control 65 (2017) 149–159, https://doi.org/10.1016/j.ijggc.2017.08.013.
[37] C. Linderholm, A. Lyngfelt, M. Rydén, M. Schmitz, Chemical-looping combustion of biomass in a 100 kW pilot, 25th European Biomass Conference and Exhibition (2017), p. 412-415. https://www.entek.chalmers.se/lyngfelt/co2/303Calle100kWbiomassEUBCE2017.pdf.
[38] A. Abad, J. Adánez, P. Gayán, L.F. de Diego, F. García-Labiano, G. Sprachmann, Conceptual design of a 100 MW$_{th}$ CLC unit for solid fuel combustion, Appl. Energy 157 (2015) 462–474, https://doi.org/10.1016/j.apenergy.2015.04.043.
[39] P. Bartocci, A. Abad, A.C. Flores, M. las Obras Loscertales, Ilmenite: A promising oxygen carrier for the scale-up of chemical looping, Fuel 337 (2023) 126644, https://doi.org/10.1016/j.fuel.2022.126644.
[40] D. Mei, A.H. Soleimanisalim, C. Linderholm, A. Lyngfelt, T. Mattisson, Reactivity and lifetime assessment of an oxygen releasable manganese ore with biomass fuels in a 10 kW$_{th}$ pilot rig for chemical looping combustion, Fuel Process. Technol. 215 (2021) 106743, https://doi.org/10.1016/j.fuproc.2021.106743.
[41] C. Linderholm, A. Lyngfelt, A. Cuadrat, E. Jerndal, Chemical-looping combustion of solid fuels – Operation in a 10kW unit with two fuels, above-bed and in-bed fuel feed and two oxygen carriers, manganese ore and ilmenite, Fuel 102 (2012) 808–822, https://doi.org/10.1016/j.fuel.2012.05.010.
[42] C. Linderholm, M. Schmitz, P. Knutsson, A. Lyngfelt, Chemical-looping combustion in a 100-kW unit using a mixture of ilmenite and manganese ore as oxygen carrier, Fuel 166 (2016) 533–542, https://doi.org/10.1016/j.fuel.2015.11.015.
[43] P. Markström, C. Linderholm, A. Lyngfelt, Operation of a 100 kW chemical-looping combustor with Mexican petroleum coke and Cerrejón coal, Appl. Energy 113 (2014) 1830–1835. https://www.sciencedirect.com/science/article/pii/S0306261913003620.
[44] M. Rydén, P. Moldenhauer, S. Lindqvist, T. Mattisson, A. Lyngfelt, Measuring attrition resistance of oxygen carrier particles for chemical looping combustion with a customized jet cup, Powder Technol. 256 (2014) 75–86, https://doi.org/10.1016/j.powtec.2014.01.085.
[45] C. Linderholm, M. Schmitz, A. Lyngfelt, Estimating the solids circulation rate in a 100-kW chemical looping combustor, Chem. Eng. Sci. 171 (2017) 351–359, https://doi.org/10.1016/j.ces.2017.05.025.
[46] G.P. Smith, D.M. Golden, M. Frenklach, N.W. Moriarty, B. Eiteneer, M. Goldenberg, C.T. Bowman, R.K. Hanson, S. Song, W.C.G. Jr., V.V. Lissianski, Z. Qin, http://www.me.berkeley.edu/gri_mech (accessed December 29, 2024).
[47] D.G. Goodwin, R.L. Speth, H.K. Moffat, B.W. Weber, Cantera: An object-oriented software toolkit for chemical kinetics, thermodynamics, and transport processes. https://www.cantera.org, 2018. Version 2.4.0. doi:10.5281/zenodo.1174508., 2018.
[48] J. Revel, J.C. Boettner, M. Cathonnet, J.S. Bachman, Derivation of a global chemical kinetic mechanism for methane ignition and combustion, J. Chim. Phys. 91 (1994) 365–382, https://doi.org/10.1051/jcp/1994910365.
[49] B. Fleiß, A. Bartik, J. Priscak, F. Benedikt, J. Fuchs, S. Müller, H. Hofbauer, Experimental demonstration of 80 kW$_{th}$ chemical looping combustion of biogenic feedstock coupled with direct CO_2 utilization by exhaust gas methanation, Biomass Convers. Biorefin. 14 (2024) 20973–20990, https://doi.org/10.1007/s13399-023-04311-9.
[50] S.R. Turns, Understanding NOx formation in nonpremixed flames: Experiments and modelling, Prog. Energy Combust. Sci. 21 (1995) 361–385, https://doi.org/10.1016/0360-1285(94)00006-9.
[51] C.T. Bowman, Kinetics of Pollutant Formation and Destruction in Combustion, Prog. Energy Combust. Sci. 1 (1975) 33–45, https://doi.org/10.1016/0360-1285(75)90005-2.
[52] T. Mattisson, A. Lyngfelt, H. Leion, Chemical-Looping with Oxygen Uncoupling for Combustion of Solid Fuels, Int. J. Greenhouse Gas Control 3 (2009) 11–19, https://doi.org/10.1016/j.ijggc.2008.06.002.
[53] A. Lyngfelt, K. Andersson, L.R. Pettersson, Design of circulation system and downstream gas treatment of a full-scale boiler for Chemical-Looping Combustion, 16th International Conference on Greenhouse Gas Control Technologies (2022). https://doi.org/10.2139/ssrn.4286370.
[54] B. Fleiß, Investigation of Chemical Looping Combustion in Fluidized Beds as Bioenergy Carbon Capture and Storage Technology, Technical University of Vienna, Wien, 2024. https://repositum.tuwien.at/handle/20.500.12708/198717.